fetal, and placental. Each of these indicators consisted of 3 or 4 conditions (e.g., fetal indicators: fetal compromise, fetal phenotype abnormality, or multiple gestations). We determined the level of concordance between clinical indicator condition and placental pathologic diagnosis.
Results: Of submitted placentas with clinical indicators (81%), 49% were maternal indicators, 31% fetal, and 19% placental. In 64% of placentas, the pathologic diagnosis correlated with the clinical indicator. The highest concordance (100%) was with the suspected condition of chorioamnionitis/infection and the lowest level of concordance (33%) was with suspected placental conditions (e.g., previa, retained products, etc.). In 19% of specimens, an appropriate clinical indicator was not provided and the majority was from women who had a Cesarean section with bilateral tubal ligation and no maternal, fetal or placental indications of disease. None of these placental specimens had significant pathologic findings. Extrapolated to the entire year, our laboratory performed a placental examination without appropriate clinical indication in 114 cases.
Conclusions: We hypothesize that a standard clinical indicator checklist may be used to triage placentas for pathologic examination. Providing clinicians with correlation of clinical indicator-pathologic findings also may be used to evaluate the utility of the clinical indicator assessment. Improved lab efficiency may be achieved by limiting unnecessary placental examinations without compromising safety.

2123 Specimen Consideration for EGFR Mutatiopnal Analysis in Non-Small Cell Lung Cancer

W Xiong, C Pritchard. University of Washington, Seattle, WA.
Background: Between 05/2010 and 02/2011, we tested 93 cliinical specimens for mutations in exons 18 to 22 encoding TK domain of EGFR, among which 9 cases failed in the PCR amplication. In this study, we attempted to examine the properties of speicmens that may contribute to failure. The findings will help clinicians and pathologists choose the optimal specimens for EGFR mutational study.
Design: For EGFR mutation testing in our institution, speimens were first tested for the common mutations, including exon 19 deletion by fragment analysis and L858R by melting curve analysis following PCR amplficaiton. Negative cases were subsequently submitted for sequencing of exon 18 to 22. All 93 cases were included in the study. The following information was documented, including pathological diagnosis, type of speicmen (FNA, biopsy, or resection), anatomical site, referring hospital, decalcification status, size of the specimen subject to test, tumor cell per centile, DNA yield, and EGFR mutation status. For the 9 failed cases, we also documented what stage the failure occured as well as the clinical outcomes.
Results: Among 93 cases, EGFR mutation was deteted in 24% of cases and no mutation was deteded in 67% of cases. 9 cases (9%) failed for the study due to insufficient DNA for PCR amplification. Among the failed cases, 1 case turned out to be breast cancer and was subsequently exlucded from the study. In terms of specimen type, cytology specimens had the highest failure rate. The anatomical sites significantly associated with test failure inlcuded brain and bone. The size of specimen in failed cases was significantly smaller than the one in the successful cases. All the failed cases had DNA yield <2ug while majority of successful cases had DNA yield >2 ug. The failure rate in specimens <5mm^3 was 15% while the failure rate was 0 in specimen >5mm^3. Interestingly, only 1 out of 5 decalcified specimens (20%). In terms of outcomes, 2 cases had additional tissue from the same procedure that were successfully tested. The remaining cases had not 2nd biopsy for EGFR testing.
Conclusions: The size of the specimen is the most important factor assoicated with failure in EGFR mutational analysis of NSCLC in our study. There is 15% failure rate if the specimen is <5mm^3. If sufficient sample is obtained (>5mm^3), the EGFR mutational analysis has 100% successful rate. The significance of delcalcification remains unclear in this relatvely small study.

2124 Validation Study of Telepathology on Frozen Section Diagnosis in a Multi-Hospital Subspecialized Pathology Department

W Yu, C Llanos, V Nose, C Gomez. University of Miami Miller School of Medicine, Jackson Memorial Hospital, Sylvester Comprehensive Cancer Center, Miami, FL.
Background: Telepathology is increasingly used for intraoperative frozen section (FS) with great accuracy. In our department, 2 rotating on-duty specialty pathologists cover FS in 3 hospitals, located about a 15-minute-walking distance from each other. Offices for the pathologists are located in 2 of the 3 hospitals. Telepathology has the great potential to improve the turnaround time (TAT) and facilitate consultation. We explored the feasibility of implementing dynamic telepathology for FS in our department.
Design: Our telepathology system includes an Olympus BX40 microscope, an Olympus DP71 camera and MicroSuite Pathology Edition software in the FS suite. Access to the internet and internet browser are the only requirements for the pathologist's computer terminal. For this study, 10 FS cases were randomly chosen by an assistant. The slides were transmitted in real time to 10 specialty pathologists by a junior resident. Short patient history and specimen site were provided. The pathologists independently evaluated each FS slide and rendered a telepathology diagnosis (TPD). Afterward, the glass slides were reviewed and each gave a light microscope diagnosis (LMD). Neither the resident nor the pathologists knew the original FS diagnoses (FSD) or the permanent section diagnoses (PSD). There were no discrepancies between the FSD and PSD.
Results: There were 100 TPD and LMD diagnoses among the 10 pathologists. The overall TPD accuracy was 97%; the LMD accuracy was 98%. For 12 of the 100 TPD responses, the diagnoses were made by pathologists who are specialists in the specimens being evaluated. For the remaining 88 TPD responses, the pathologists were evaluating specimens outside their specialty areas. Nine out of 88 diagnoses (10%) made by specialists outside their own specialty area included diagnoses that were less specific, requested additional tissue or deferred the diagnosis to permanent sections. This did not occur for any of the 12 diagnoses (0%) made by the pathologists in their specialty area.
Conclusions: The diagnostic accuracy of telepathology for FS is good (97%), similar to the conventional method (98%). Therefore, it appears to be a valid alternative, especially when there is an emergent situation to improve the TAT. Additionally, the specialists' diagnoses within their specialty area are more specific and well-defined. Therefore, by facilitating consultation, telepathology holds the promise to improve the overall FS diagnostic accuracy with minimal delay of the TAT.

2125 Large Specimen Surgical Pathology Reporting Facilitated by Lean Workflow and Rapid-Cycle Microwave Processor

RJ Zarbo, RC Varney, MJ Dib, B Mahar. Henry Ford Hospital, Detroit, MI.
Background: Timeliness of pathology reporting is one of the most common challenges in Surgical Pathology, particularly for large and complex specimens resections requiring more intensive workup for diagnosis. This even more challenging for teaching institutions that integrate residents and education into a large specimen dissection service and can be compounded by Core Histology Laboratory operations that serve as central processing units for numerous remote hospitals.
Design: Pathology workflow in the Henry Ford Hospital Surgical Pathology and Histology Core Laboratory was optimized for continuous flow from work processes of accessioning through gross dissection, histology tissue processing, slide cutting and delivery to pathologists. In this work system, we tested integration of a rapid-cycle microwave processor (Logos, Milestone Medical, Kalamazoo, MI) into continuous flow work for large specimens. The isntrument was initially validated for processing times according to submitted specimen thicknesses from 1-3mm. All specimens were dissected fresh with occurrence of both fixation and processing on the instrument for total processor times ranging from 1.25-3 hours. We then compared surgical pathology report TAT from our previous July 2011 condition of overnight processing of large specimens to the new August 2011 condition of continuous flow processing of larger/complex specimens corresponding to CPT codes 88307 and 88309. Specimen dissection was performed by pathologists' assistants and residents.
Results: 37 large specimen cases (33 coded as 88307 and 4 coded 88309) were dissected fresh at 3mm thickness with formalin fixation and processing in continuous flow on the rapid-cycle processor. TAT from time of accession to case signout was 3.2 days. This is a reduction of 36% from the previously attained TAT of 5 days for both large specimen classes of 88307 and 88309. No histology processing or slide stain quality defects were observed.
Conclusions: Efficient work system designs in surgical pathology and histology can be enhanced with integration of rapid-cycle processors that promote the proven Lean efficiency concept of continuous flow. In teaching institutions, quality and consistency of the work product requires a gross dissection discipline by pathology residents and a different approach that shrinks the non-value added time waste associated with historical overnight or late afternoon batch mode gross dissection.

Techniques

2126 Effects of Long Term Tissue Fixation on the Immunohistochemical Expression of MSI Makers in Colon Adenocarcinoma

P Adegboyega. LSU Health Sciences Center, Shreveport, LA.
Background: Colorectal adenocarcinomas with microsatellite instability (MSI) do not respond well to Fluorouracil-based chemotherapy and do have treatment outcome that differs from that seen in microsatellite stable tumors. In clinical settings, immunohistochemical staining for makers of MSI [Mismatch repair (MMR) gene products] is used to screen for the presence of MSI; and has been shown to have comparable sensitivity and specificity with MSI detection by PCR. It was recently shown that routinely used tissue fixative such as dissect aid negatively impacts MMR proteins immunohistochemistry. 10% Neutral Buffered Formalin (NBF) was shown to be the optimal tissue fixative for MMR protein immunostaining in routine surgical pathology practice. This study explores the effects of long term NBF tissue fixation on the immunohistochemical expression of three MMR gene products (MLH1, MSH2 and MSH6).
Design: Study materials consisted of cases of colonic adenocarcinoma: 7 primary colectomy and 1 secondary hepatectomy specimens received for tumor diagnosis and staging. Samples of normal colon and tumor from each specimen were fixed in NBF and submitted for routine processing with paraffin embedding after fixation for 1 day, 1 month, 3 months, 6 months and 1 year. Immunohistochemistry for MLH1, MSH2 and MSH6 was performed on representative sections of each block. Immunoreactivity scoring was done using a semi-quantitative score of 0, 1, 2, 3 and 4.
Results: MLH1 immunoreactivity scores for all the samples were strong for the samples within the first 3 months of fixation (previous findings) but thereafter became drastically reduced and is completely negative in 5 of 8 cases for MLH1, 3 of 8 cases for MSH2 and 2 of 8 cases for MSH6 after one year of fixation.
Conclusions: Although 10% Neutral Buffered Formalin solution is the preferred fixative for MMR immunohistochemical assay, long term tissue fixation (greater 3 months) results in loss of immunoreactivity of MMR proteins in tissue sections and so may produce spurious results (false MSI status).

2127 Detection of KRAS Mutations by Locked Nucleic Acid PCR Sequencing in Pancreatic Cyst Fluid Cells

CE Aguilar, AL Moreira, H Gerdes, M Ladanyi, K Nafa, CS Sigel. Memorial Sloan-Kettering Cancer Center, New York.
Background: Mutation of *KRAS* is one of the earliest alterations in pancreatic adenocarcinoma (PA). As such, in combination with clinical and cytologic findings, detection of *KRAS* mutations may have a role in the pre-operative management of

pancreatic cysts. As of yet, detection by standard methods has shown suboptimal sensitivity possibly due to low levels of the mutant alleles in cyst fluid. We evaluated a locked nucleic acid (LNA) PCR sequencing assay to detect low levels of mutant *KRAS* DNA in pancreatic cysts.

Design: DNA was extracted from 32 pancreatic cyst fluid cell pellets (CFP) and 20 formalin-fixed paraffin embedded (FFPE) cell block and resection samples (CB/RS) using a DNA extraction kit. Resection samples were routinely macro-dissected to enrich for tumor. LNA-PCR was performed in the presence of an LNA oligonucleotide that suppresses the amplification of the wild type *KRAS* exon 2 DNA, leading to preferential amplification of any mutant alleles. The PCR products of both standard and LNA-PCRs were purified and sequenced.

Results: Standard Sanger sequencing detected 8 *KRAS* mutations (8/32; 25%) from CFP; LNA-PCR detected an additional 7 mutations (7/28; 56%). Thirteen cases were negative by both methods (41%). LNA-PCR was not available in 4 cases. Analysis of corresponding FFPE CB was concordant with CFP in 8/9 cases (89%) by both methods; LNA-PCR detected one additional mutation. Of 11 paired CB/RS archived samples evaluated by both methods, all CB were KRAS negative and 3/11 RS (27%) were KRAS positive. KRAS positive cases (6/20) included intraductal pancreatic mucinous neoplasms (IPMN) (2) with low or high grade dysplasia, mucinous PA, metastatic PA, minimally invasive PA arising with IPMN, and poorly differentiated carcinoma, while KRAS negative cases included an IPMN with moderate dysplasia (1), serous cystadenoma (5), solid pseudopapillary neoplasm (1), low grade well-differentiated cystic endocrine neoplasm (3), benign retention cyst (1), and para-ampullary duodenal cysts involving pancreas (1).

Conclusions: The management of patients with pancreatic cysts requires integration of clinical, radiologic, and pathologic findings. We find that high sensitivity LNA-PCR detects more *KRAS* mutations than standard PCR, increasing the usefulness of *KRAS* mutation analysis in the evaluation of low cellularity specimens, further raising diagnostic accuracy.

2128 Splenic Manifestation of Chronic Autoimmune Disease: A Report of Five Cases with Histiocytic Necrotizing (Kikuchi-Fujimoto-Like) Change in Four Cases with Use of 16s rDNA PCR To Exclude Infection

NS Aguilera, TA Summers, B Zhang, A Auerbach. Joint Pathology Center, Silver Spring, MD; Walter Reed National Medical Center, Bethesda, MD; Henry Jackson Foundation, Gaithersburg, MD.

Background: Autoimmune diseases are often associated with enlarged lymph nodes and splenomegaly. The histologic findings in splenic white pulp and lymph nodes have been commonly described as follicular hyperplasia. Histiocytic necrotizing lymphadenopathy has also been described in autoimmune disease, but a similar counterpart in the spleen has not been documented.

Design: Five splenectomy specimens associated with autoimmune disease were retrieved from our files. An immunohistochemical panel for CD3, CD8, CD20, CD68, lysozyme, CD123, CD163, IgG4, Hemoglobin peroxidase, myeloperoxidase, kappa and lambda was performed in 4/5. Stains for infectious organisms and in situ hybridization for EBV (EBER) were also performed. A 16S rDNA PCR was performed on FFPE DNA samples isolated from 4/5 cases. The universal primer set [27f/1492r] targeting 16S rRNA gene for most eubacteria was applied to the assay. Clinical data was obtained in all cases.

Results: Patients were 24 to 56 yrs old (mean 40 yrs; M:F-3:2). 3/5 had SLE; 1/5 RA; 1/5 L.E prep + and ANA+. All had splenomegaly 232 -803gm (mean 421 gm). 4/5 exhibited histiocytic necrosis without acute inflammation similar to Kikuchi-Fujimoto disease. 4/5 showed extramedullary hematopoiesis. 1/5 showed florid follicular hyperplasia with little necrosis. Splenic involvement was focal to diffuse. The white pulp showed necrosis with karyorrhectic debris. Surrounding the necrotic areas were benign histiocytes and immunoblasts. Plasma cells were present; IgG4 was not increased. Hematoxylin bodies and CD123+ plasmacytoid dendritic cells were not identified. Stains for infectious organisms were negative. IHC Kappa and lambda showed no clonality in 4/4. EBER stained rare single cells in 4/4 cases tested. The 16S rDNA assay was negative (no amplification) in 2/4 cases and equivocal in 1/ 4 (1 in 7 blocks amplified).

Conclusions: Splenomegaly in autoimmune disease is rarely studied and is thought to be hyperplastic in most cases, but we present rare cases of histocytic necrosis in the spleen associated with autoimmune disease. The significance of the rare EBV positive cells in these cases, bystander or an intimate to the etiology of the splenomegaly, is uncertain. The significance of positivity in the 16SrDNA assay in one case is also uncertain and exposure to bacteria cannot be excluded.

2129 An Informatics Supported Tissue Banking Inventory and Operational System for Anatomic Pathology. Biospecimen Inventory and Operations System (BIOS): An Update

W Amin, A Vemulapalli, L Mock, M Bisceglia, R Dhir, AV Parwani. University of Pittsburgh, Pittsburgh, PA; University of Pittsburgh Medical Center, Pittsburgh, PA.

Background: To meet the growing need of annotated biospecimen and manage the daily operation of tissue bank UPMC has developed BIOS that is designed for a high-quality, well annotated biospecimen management for tissue bankers, clinicians and researchers needs. It provides a robust query and management capability that eventually allows biobanker to identify the biospecimens to meet the needs of the research community.

Design: BIOS is a Microsoft. NET web application with s SQL reporting services for adhoc reporting needs. It combines the efforts of tissue collection, patient consents status, billing and data aggregation in one module. It links to Medipac for accurate importing of patient demographics. It also has the functionality to build custom queries and export data into either PDF or excel formats. The system has inbuilt with HIPAA logging functionality with every step logged into database. It provides form based security that is implemented to validate user access to multiple modules. Patient information is de-identified for some user roles and access is maintained through Active Directory.

Results: The BIOS system has been successfully implemented at our institute and is currently being used for the day to day operations of a system-wide tissue bank. It holds 19500 patients and 123732 specimen information. There are 19 active user at University of Pittsburgh Medical Center tissue bank. It provides a central repository for the tissue bankers for tracking and distribution of biospecimens and for robust querying and reporting of biospecimens and associated data to fulfill the requirements of clinical translational researchers.

Conclusions: BIOS in provides a central biorepository to access information on multimodal data sets and the ability for tracking and integration with other limbs of a tissue bank. In addition BIOS provides the tissue bankers with a robust, queryable, and maintainable system that can be integrated with other tissue banking and pathology tools including image and molecular data integration. Furthermore, this model can be successfully deployed at other institutions as well.

2130 Image Analysis and Next Generation Sequencing: Strange Bedfellows for Quality Assurance of *KRAS* Mutational Status in Colorectal Cancer

JP Baliff, Z-X Wang, SC Peiper. Thomas Jefferson University, Philadelphia, PA.

Background: The interface between anatomic pathologists and the molecular pathology laboratory is increasingly important with the development of oncologic therapies with companion diagnostics for solid tumors. One critical step in mutational analysis for *KRAS*, *BRAF*, and *EGFR* is the identification of tumor on a H&E slide, with tumor burden meeting analytical sensitivity to avoid false negatives. This process can be difficult when tumor content is low (e.g. biopsy specimens). Deep sequencing using Next Generation sequencing (NGS) is very accurate in quantifying the relative content of mutated and normal alleles in amplicons from tumor specimens. Using NGS as the gold standard, we assess if image analysis of tumor slides can be an objective and reliable method to provide quality assurance (QA) for mutation analysis.

Design: Specimens were selected from archives based on diagnosis of colonic adenocarcinoma and known positive *KRAS* mutation status by Sanger sequencing. A H&E stained slide with encircled tumor was scanned into an Aperio ScanScope digital scanner (Vista, CA) and image analysis to identify tumor cells, mucin, necrosis, and stroma performed within the circled region by both surface area and nuclear count. DNA was extracted from within the identical encircled area and exon 2 of *KRAS* was amplified by PCR and sequenced using a 454 Junior pyrosequencer (Roche, Branford, CT). 5 barcoded samples were sequenced in each run yielding 10,000-20,000 reads/case, equally distributed between forward and reverse reads. Correlation between the percentage of tumor calculated by image analysis compared to that from NGS was determined.

Results: 7 cases of *KRAS* mutated colorectal cancer were selected for analysis. NGS detected identical *KRAS* mutations as previously found by Sanger sequencing. In tumors containing large areas of necrosis, image analysis of surface area consisting of tumor and necrosis best correlated with mutated DNA by NGS. When minimal necrosis existed, image analysis by nuclear count was equivalent to surface area in the correlation with mutated DNA by NGS.

Conclusions: The amount of tumor present on a slide by image analysis serves as a QA verification of the relative content of mutations derived by NGS. Virtual microscopy may be incorporated into the workflow of the molecular laboratory to correlate the content of tumor cells with the relative content of specific mutations. This approach will be of clinical utility in the analysis of small specimens as well as those with limited numbers of tumor cells.

2131 Molecular Diagnostic Analysis of Supernatant Fluid from Fine Needle Aspirate, Bile Duct Brushing and Effusion Cytology Specimens

WW Bivin, JF Silverman, SD Finkelstein, Y Liu, A Mohanty, B Ujevich, C Binkert, U Krishnamurti. Allegheny General Hospital, Pittsburgh, PA; RedPath Integrated Pathology, Inc., Pittsburgh, PA.

Background: Fine needle aspiration (FNA), bile duct brushing and body cavity fluid specimens can be limited by low cellularity and sampling variability. Molecular analysis can complement the cytologic findings in challenging cases. In this study we evaluated a novel technique performing DNA mutational profiling on the cytocentrifugation supernatant fluid collected during cytology preparation but is usually discarded.

Design: A variety of cytology specimens (45 FNAs of solid organs, 10 pancreatic/biliary duct brushings and 23 body cavity fluids) underwent standard cytology processing which included centrifugation to separate cells of interest. DNA was extracted from 2 ml of the centrifugation supernatant fluid. DNA quantity was measured by optical density and quality by qPCR. Mutational analysis followed using PCR/capillary electrophoresis for a broad panel of markers (KRAS point mutation by sequencing, microsatellite fragment analysis for loss of heterogeneity of 16 markers at 19, 3p, 5q, 9p, 10q, 17p, 17q, 21q, 22q). Microdissection of corresponding stained cytology smears and/or cytocentrifugation cellular slides were similarly analyzed and compared.

Results: In each organ system and sampling format, the cell-free supernatant fluid contained adequate levels of amplifiable DNA for analysis. Known non-neoplastic specimens (n=58) did not show false positive detection of mutations. In contrast, all positive malignant specimens had detectable mutational change. There was a high degree of mutational profile concordance for mutations detected in the microdissected stained cytology. More importantly, mutation detection was consistently superior in the supernatant fluid (mean 6.7 mutations) compared to that in the microdissected cells (mean 4.2 mutations, $p<.001$), both in number of total mutations as well as extent of mutation clonality.

Conclusions: 1.) Centrifugation supernatant fluid provides for an abundant and robust source of DNA for molecular analysis. 2.) The greater extent and clonality of detectable mutational change in the supernatant fluid supports it being enriched with

neoplastic DNA when cancer is present. 3.) Mutations detected in the supernatant fluid are concordant with that detected in neoplastic slide based cells. 4.) All these findings make the supernatant fluid a reliable source for mutational analysis and helps overcome the limitations of low cellularity and sampling variability in FNA biopsy, bile duct brushing and effusion cytology specimens.

2132 Diagnostic Tissue Preparation: Further Assessment of Microwave-Based Compared to Conventional Tissue Processing

CR Blieden, MC Reyes, MT Garcia-Buitrago, V Nose, S Vernon, AR Morales. University of Miami/Jackson Memorial Hospital, Miami, FL; Memorial Sloan-Kettering, Miami, FL.

Background: Rapid tissue processing (RTP) has changed tissue preparation. Compared to conventional vacuum infiltration processing (VIP), RTP reduces turn around time, patient anxiety, and conserves laboratory resources. Despite this, there has been some unwillingness to use RTP as opposed to VIP. Our goal was to determine if pathologists at various levels of training and academic appointment could discern among preparations using RTP and VIP. Additionally, we investigated the effect of reagent deterioration with both methods of tissue processing with both machines.

Design: Tissue was collected from a variety of surgical specimens fixed in 10% neutral buffered formalin. Two groups of 1500 specimens were processed with different reagent compositions by RTP (A and B respectively); one group of 1500 specimens was processed via VIP. All sections were prepared by the same histotechnologist. Samples from the initial, middle, and end phase of the cycles were taken. A total of 90 slides (30 from each interval) from each of the three groups were analyzed by five individuals at various stages in their careers; a second year resident, a fellow, an assistant professor, an associate professor, and a tenured professor. Reviewers were instructed to rate the quality of sections from 1 (best) to 3 (worst) and to indicate whether or not they could distinguish the section processed via VIP. The type of machine used to process each section was not revealed to the reviewers.

Results: Cumulative results were as follows: For solution A using RTP, 366 slides were given a grade 1, 77 were given a grade 2, and 7 were given a grade 3. For solution B using RTP 354 slides were given a grade 1, 80 were given a grade 2, and 16 were given a grade 3. For CP, 372 were given a grade 1, 73 were given a grade 2, and 5 were given a grade 3. For all three groups, there was no significant difference in grades for the three time intervals, indicating that reagents did not deteriorate over the course of 1500 sample batches for any group.

Conclusions: All reviewers produced similar results. There was no difference in quality among two RTP groups and the VIP. This study further validates the quality of rapid tissue processing compared to conventional methods. The advantages of rapid tissue processing (continuous sample loading, less reagent expenditures and toxicity, and identical quality of histologic preparation when compared with conventional methods) further endorses the use of the RTP among laboratories in all clinical practices.

2133 The Cytocentrifugation of Supernatant Fluid from Thyroid Nodule Fine-Needle Aspirates Provides Analyzable DNA Suitable for Molecular Analysis

SJ Bokhari, JF Silverman, SD Finkelstein, U Krishnamurti, Y Liu, B Ujevich, C Binkert, A Mohanty. Allegheny General Hospital, Pittsburgh, PA; RedPath Integrated Pathology, Pittsburgh, PA.

Background: Thyroid fine needle aspiration (FNA) biopsy specimens can be among the more challenging specimens in cytology to reach a definitive diagnosis due to the often subtle and overlapping features of non-neoplastic (hyperplasia), benign (follicular adenoma) and malignant (follicular and papillary carcinoma) neoplasms. Molecular targets for specific lesions (point mutation, translocation, loss of heterozygosity) are known. Therefore, our study focused on a pilot assessment to determine whether the cell-free part of the FNA sample would have sufficient free DNA for molecular analysis, possibly aiding in the differentiation of the aforementioned classes of thyroid lesions, while at the same time submitting the available cellular material for cytologic examination.

Design: Smears and cytocentrifugued FNA needle-rinsings from 16 thyroid nodules were studied. DNA was extracted from 2 ml of the cytocentrifugation supernatant fluid and the DNA quantity/quality measured by optical density/qPCR. Mutational analysis was performed using PCR/capillary electrophoresis for a broad panel of markers (KRAS, BRAF point mutation by sequencing, microsatellite fragment analysis for loss of heterozygosity(LOH) of 16 markers at 19, 3p, 5q, 9p, 10q, 17p, 17q, 21q, 22q). Microdissection of stained cytology smears and/or cytocentrifugation cellular slides were similarly analyzed and compared.

Results: All thyroid FNA needle-rinse fluids contained abundant amplifiable DNA suitable for broad panel mutational analysis. The DNA level in the cell-free supernatant rinse fluid ranged from 3.7-83.9 ng/ul; DNA level in the supernatant did not necessarily correlate with morphologic assessment of smear cellularity. Oncogene point mutations and LOH allelic imbalance mutations present in the microdissected cells of the stained cytology smears were also identified in all corresponding cell-free needle rinse supernatant fluids. Of note, the DNA level was higher in malignant nodules (mean 47.2 ng/ul) compared to non-neoplastic disease (mean 12.4 ng/ul).

Conclusions: The cytocentrifugation supernatant fluid of thyroid FNA specimens contains adequate levels of amplifiable DNA for broad panel mutational analysis in both the cellular and paucicellular specimens. The cytocentrifugation supernatant fluid, currently not utilized, is available for complementary molecular analysis, and could provide additional useful information, especially in equivocal cases.

2134 Improved Detection of the BRAF c.1799T>A (p.V600E) Mutation in Melanoma with a Single Nucleotide Primer Extension Assay

GC Caponetti, E Racila, A Stence, J Pruessner, S Forde, J Hackman, D Ma, J Heusel, A Bossler. University of Iowa Hospitals and Clinics, Iowa City, IA.

Background: *BRAF* mutations have been identified in approximately 66% of melanomas. The most common *BRAF* mutation is the c.1799T>A on exon 15 with the resultant p.V600E. Melanoma patients bearing this mutation can significantly benefit from vemurafenib therapy. Sanger sequencing (SS) is the most commonly used test for the detection of this mutation. However, its analytical sensitivity is only 20% in formalin-fixed paraffin-embedded (FFPE) tissue. Therefore, it is crucial to identify a more sensitive method. In addition, melanin is known to inhibit Taq polymerase activity. The aims of this study were to determine the analytical sensitivity of a Single Nucleotide Primer Extension (SNPE) assay for the detection of the *BRAF* c.1799T>A mutation in melanoma and assess the impact of endogenous melanin on the performance of both assays.

Design: Genomic DNA (gDNA) was extracted from FFPE tissue of 21 melanoma cases. The SNPE assay was performed using the ABI PRISM® SNaPshot® kit (Applied Biosystems, Carlsbad, CA) in parallel with bi-directional SS. The analytical sensitivity of the SNPE assay was determined using purified plasmids containing the *BRAF* c.1799T>A (p.V600E) mutation at limiting dilutions admixed with 25 ng of wild type gDNA. The percentage of melanin content in the cases of melanoma was assessed by histological review.

Results: The analytical sensitivity of the SNPE assay was as low as 2%. In 24% (n=5) of the cases, the SS reaction failed but the SNPE was able to identify the mutation. Only one SNPE reaction failed. In cases with initial failure of the SS reaction, the average melanin content was 38% (ranging from 1% to 90%). A significantly lower melanin content (0% to 40%, average 15%) was seen in cases with successful sequencing. By diluting the DNA or re-sampling of an area of tumor with less melanin, we were able to successfully perform SS in all the cases that had initially failed.

Conclusions: Although the number of cases analyzed in this series is small, our findings suggest that the prevalence of the *BRAF* c.1799T>A (p.V600E) mutation in melanoma can be underestimated due the intrinsic limitations of SS and its susceptibility to interference by melanin. The SNPE assay is a much more sensitive alternative for the identification of this mutation and less susceptible to interference by melanin. The development of a multiplexed SNPE assay for the identification of other *BRAF* mutations appears promising and is currently being evaluated.

2135 Application of Design of Experiment (DOE) Principles to the Development of Biologic Control Materials in Immunohistochemistry

J Erickson, D Huang, M Hudson, S Webster. Dako North America, Inc., Carpinteria, CA.

Background: Cell lines with specific antigen expression levels are useful controls for qualifying immunohistochemical (IHC) staining runs. To successfully fulfill this function embedded cell pellets must exhibit the desired level of antigen expression and do so in a robust and reproducible manner. The use of DOE methods and 2^k factorial experiments supported by image analysis is an efficient and objective way to optimize the manufacture of these control materials.

Design: To illustrate the DOE approach, key process variables were examined for their effects on the IHC staining intensity of paraffin-embedded HT-29 (colorectal adenocarcinoma) cultured cells. Section thickness and humidity in the drying oven were analyzed in a 2^2 factorial design, and as a more complex example fixation and dehydration times were examined with embedding matrix type in a 2^3 factorial experiment. Relative antigen expression levels were estimated using the ACIS® III slide scanner (Dako) and an image analysis algorithm based on staining intensity. Data were evaluated using Minitab® statistical software.

Results: The 2^2 experiment demonstrated decreased staining intensity with higher humidity (p=0.001) and a nonsignificant trend with thinner section thickness (p=0.152). Higher humidity was also associated with increased variability in intensity and compromised cell-to-slide adherence. The 2^3 experiment produced significant increases in staining intensity, in this case with increased fixation time (p=0.039) and the use of Type 2 embedding matrix (p=0.000) but not with change in dehydration time. Interestingly, there were two significant interactions between variables. Decreased fixation time lowered staining intensity with the use of Type 1 but not Type 2 embedding matrix (p=0.032) and increased fixation increased intensity with shorter dehydration periods but not with longer periods. Thus, DOE methods effectively reveal the impact of process variables (alone and in combination) on both the magnitude and variation of the response variable.

Conclusions: DOE and factorial experiments provide a systematic way of analyzing processes and optimizing key parameters to achieve a specified result, i.e. a robust and reproducible manufacturing protocol. The use of image analysis complements the DOE approach as it provides an objective scoring method and produces parametric data that are amenable to statistical analysis. It is important to note that each cell line control should be investigated individually as the effects of the manufacturing processes may be assay-specific.

2136 Vascular Leak Is a Central Feature in the Pathogenesis of Systemic Sclerosis

TM Frech, MP Revelo, SG Drakos, MA Murtaugh, B Markewitz, AD Sawitzke, DY Li. University of Utah, Salt Lake City.

Background: Systemic Sclerosis (SSc) is a multi-organ system disease characterized by activation of immune cells, production of auto-antibodies, microvascular changes, and fibrosis. Clinical studies suggest that there are three classic stages of SSc: edematous, fibrotic, and atrophic. Definition of microvascular changes occurring during this early edematous phase prior to the development of fibrosis is of utmost importance. Whole-

field digital microscopy offers a means of rapidly carrying out quantitative, reproducible measurements of micro-anatomical features in high-resolution pathology images and in large image datasets with control for intra-observer and inter-observer variability. As such, its use for systematic examination of subtle differences exhibited by diseased tissue has potential to improve the characterization of the histologic stage, prognosis, and treatment responses.

Design: Twenty consecutive SSc patients were biopsied on the left or right medial forearm with a 6 mm punch biopsy. Biopsy specimens in the same location were obtained from 4 healthy controls. These specimens were processed with hematoxylin and eosin, histochemical and immunohistochemical stains. Wholefield digital microscopy was used to grade vascular abnormalities.

Results: Whole-field digital microscopy of SSc skin biopsies revealed that endothelial abnormalities are a universal feature regardless of clinical features and/or duration of disease. These features were not seen in the healthy control specimens and did not vary with disease characteristics. Wholefield digital microscopy identified interstitial edema (29.3 ± 9.7%, p = 0.03) and fibrosis (75.4 ± 5.4%, p =0.01) in all SSc patients. The presence of hand/finger edema significantly correlated with less fibrosis on skin biopsy specimens (Spearman correlation -0.50; p=0.02). Perivascular and interstitial infiltrate of mast cells were present in all SSc specimens.

Conclusions: Whole-field digital microscopy offers a means of rapidly carrying out quantitative, reproducible measurements of microscopic features of SSc microvascular change and should be integrated into SSc research and clinical care. The universal morphologically abnormal endothelial cells and interstitial edema in all SSc patients who were biopsied regardless of their clinical characteristics suggests that SSc may be an intrinsic disease of the endothelium with fibrosis as the result of antecedent vascular leak.

2137 Interobserver Variability in the Quantification of MIB-1 Labeling Index on Cytologic Samples from Well Differentiated Neuroendocrine Tumors (WDNETs) of the Pancreas (P) and Gastrointestinal Tract (GIT): A Comparative Analysis of Three Methods

AD Fung, C Cohen, S Kavuri, X Gao, MD Reid. Emory University School of Medicine, Atlanta, GA; Georgia Health Sciences University, Augusta, GA.

Background: WDNETs of the P and GIT are classified in part by measuring MIB1 index. We determined the level of interobserver variability among 3 observers in the calculation of MIB1 labeling index by counting positive cells/400 tumor cells and doing eyeball estimation of MIB1 percentage (%) in 22 WDNETs to determine reliability/reproducibility of both tests compared to the automated cellular imaging system (ACIS, Dako).

Design: Twenty-two WDNETs of the P (n=13), GIT (n=4) and 5 liver metastases (2 colonic, 3 from P) were confirmed by cytology and immunohistochemistry. These were stained with MIB1 antibody (1;160 dilution, Dako, Carpinteria, CA). Number of MIB1-positive cells/400 tumor cells was calculated by 2 cytopathlogists (MR, SK) and 1 fellow (AF). In addition, the 3 reviewers did an eyeball estimate of MIB1% and scored cases into 3 categories; < 2%, 3-20% and > 20%. Statistical analysis using Spearman's correlation coefficient for all observers and methods was performed and compared to that obtained by ACIS.

Results: There was strong statistically significant correlation among observers when calculating MIB1-positive cells/400 tumor cells and when doing an eyeball estimate of MIB1%.

MIB1-Positive Cells/400 Tumor Cells

Observer	CC	95% CI	p-value
AF vs SK	0.83	(0.63, 1.0)	<0.05
AF vs MR	0.95	(0.88, 1.0)	<0.05
SK vs MR	0.88	(0.73, 1.0)	<0.05
"Eyeball" Estimate of MIB-1 Index			
Observer	CC	95% CI	p-value
AF vs SK	0.75	(0.48, 1.0)	<0.05
AF vs MR	0.86	(0.69, 1.0)	<0.05
SK vs MR	0.79	(0.55, 1.0)	<0.05

CC, correlation coefficient; CI, confidence interval.

Additionally when both methods were compared there was also strong (statistically significant) correlation between them. However when ACIS was compared to MIB1-positive cells/400 tumor cells and to eyeball estimation there was a weaker, albeit statistically significant, correlation between the 3 methods.

Comparison Of Methods

Method	CC	95% CI	p-value
MIB1/400 vs Eyeballing	0.78	(0.53, 1.0)	<0.05
MIB1/400 vs ACIS	0.53	(0.14, 1.0)	<0.05
Eyeballing vs ACIS	0.62	(0.23, 1.0)	<0.05

CC, correlation coefficient; CI, confidence interval.

Conclusions: The counting of MIB1-positive cells/400 tumors cells and eyeball estimation of MIB1 labeling index showed strong interobserver correlation. This would suggest that based on WHO recommendations both of these methods are more reliable and reproducible for grading of WDNETs of P and GIT on cytology samples, than ACIS.

2138 Whole Genome SNP Array Analysis Is Complementary to Classical Cytogenetic Analysis in the Evaluation of Lymphoid Proliferations

SE Gibson, J Luo, M Sathanoori, R Parikh, GK Michalopoulos, SH Swerdlow. University of Pittsburgh School of Medicine, Pittsburgh, PA.

Background: Cytogenetic evaluation of lymphoid proliferations in clinical practice relies primarily on directed FISH studies and, for a more global analysis, classical cytogenetic karyotypes (CCG). More recently, array CGH and single nucleotide polymorphism (SNP) array analyses have been used to demonstrate additional clinically relevant abnormalities. However, whether these high throughput platforms could replace CCG in the assessment of numerical chromosomal abnormalities is uncertain.

Design: After excluding 4 cases with inadequate DNA, 27 frozen lymph node and related tissue samples with available CCG studies (6 benign, 8 follicular lymphomas, 7 diffuse large B-cell lymphomas, 6 other B-cell lymphomas [ML]) were analyzed using the Genome-Wide Human SNP Array 6.0 (Affymetrix, Santa Clara, CA) and Partek Genomics Suite (Partek, St. Louis, MO). Normal copy number variations were excluded using the Database of Genomic Variants. A benign nasopharyngeal biopsy with numerous unexplained copy number alterations (CNA) and normal CCG was excluded from further analyses.

Results: 9/26 cases (5 ML, 4 benign) had a normal karyotype with CCG and SNP analysis. 8/26 cases (all ML) were partially concordant -- 1 had CNA and balanced translocations by CCG not seen with SNP analysis, 2 had additional CNA by SNP analysis, and 5 had additional, non-overlapping abnormalities by SNP analysis and CCG. 9/26 cases (8 ML, 1 benign) were discordant -- 6 had CNA by CCG not seen with SNP array, including 4 cases also with balanced translocations, and 3 cases had non-overlapping CNA by CCG and SNP analysis. SNP analysis confirmed whole chromosome gains or losses detected on CCG in 2/16 cases, and partially identified whole chromosome abnormalities in 6/16 cases. The remaining 8 discrepant cases had 55.6±31.9% abnormal metaphases. In 5 cases SNP analysis helped to clarify selected CCG findings. Deletion 6q23.3 and gain of 17q23.1-q23.2, seen in 2 ML each, were the most common additional abnormalities detected by SNP analysis.

Conclusions: Whereas SNP analysis provided information not apparent by CCG in 10 cases, CCG provided CNA data not seen in SNP analysis in 15 cases, as well as identifying balanced translocations in 11 cases. Therefore, while SNP analysis provides additional information and can help to clarify CCG findings, CCG studies remain of great utility in identifying global CNA in addition to demonstrating chromosomal translocations. Additional investigations are required to improve high throughput cytogenetic strategies and for validation of SNP array findings.

2139 Novel Quantitative Image-Analysis Based Scoring Technique for In-Situ Assessment of mRNA in Archival Tumor Tissues: Strong Correlation between Manual and Automated Schemes

JC Hanson, TR Holzer, AD Fulford, RJ Konrad, A Nasir. Eli Lilly & Co., Indianapolis; Laboratory for Exp Medicine, Indianapolis, IN.

Background: We developed a semi-quantitative scoring technique for manual *in-situ* mRNA quantification of oncology biomarkers in archival tumor tissues. We also developed an image analysis-based quantitative algorithm as an automated *in-situ* mRNA evaluation tool. The goal was comparative evaluation of these scoring techniques for novel oncology biomarkers.

Design: Archival sections from 6 non-small-cell lung carcinomas (NSCLCA) were stained for BIRC5 (survivin) mRNA. The *in-situ* mRNA staining was manually scored by an experienced pathologist as 0, 1+/2+ (<50%/≥50% area of the cell with non-confluent fine, red granules) or 3+/4+ (with partial/total confluence of granules). The sum of weighted mRNA scores (staining scores X respective %ages) was reported as a semi-quantitative (sq-) m-RNA score. Whole slide images were captured (Aperio Scanscope XT) and analyzed by Definiens' EII software. Each tumor section was scored using the manual criteria above and a quantitative (q-) m-RNA score was derived. Both scores (range 0-400) were correlated (Pearson test; GraphPad, Prism).

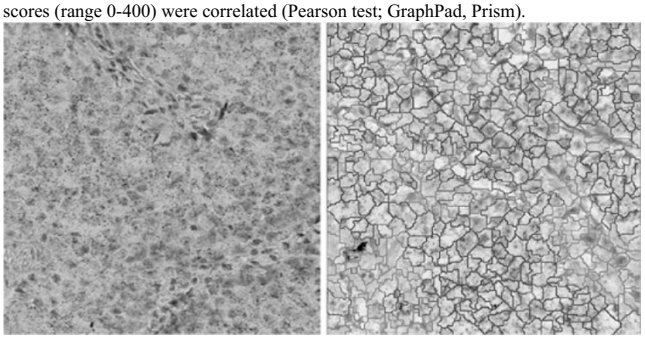

Results: Manual sq-RNA scores on 6 NSCLCA cases ranged 0-162. The automated algorithm analyzed tens of thousands of cells/section. The positive cells ranged from 2.5% to 75%, and the q-RNA score ranged from 2-120. Key challenges with the automated technique were delineation of various tissue/tumor components and tissue artifacts. The image analysis-based q-RNA scores correlated welll with the manual scores (Pearson's correlation coefficient of 0.967; p=0.002).

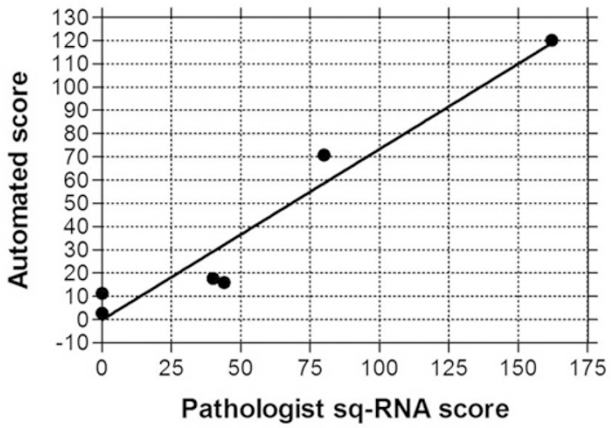

Conclusions: Our quantitative image analysis-based *in-situ* mRNA scoring on archival tumor tissues shows high-correlation with the manual techniqe. Evaluation on larger cohorts of independent test sets of archival tissues will further substantiate its practical utility in oncology clinical trials and practice.

2140 Mutational Screening in *KRAS, BRAF, EGFR, C-KIT* and *PDGFRa* in Colorectal Carcinoma (CRC) and Non-Small Cell Lung Cancer (NSCLC) Using Next-Generation Sequencing (NGS)

T Hinrichsen, O Wachter, B Dockhorn-Dworniczak, H-G Klein. Center for Human Genetics and Laboratory Medicine Dr. Klein and Dr. Rost, Munich, Bavaria, Germany; Dept. of Pathology, Kempten, Bavaria, Germany.

Background: Treatment with monoclonal antibodies (mAB) or "small molecules" (e.g. tyrosine kinase inhibitor, TKI) depends on the mutational status of certain genes in the tumour tissue of solid tumours. In CRC, the mutational status of *KRAS* and *BRAF* correlates with a response to mABs, in NSCLC the mutational status of *EGFR* and *KRAS* correlates with a benefit to TKI treatment. Other important genes in gastrointestinal stromal tumour (GIST) are *c-KIT* and *PDGFRa*. With NGS, is likely to improve the diagnostics in solid tumours. Discrete templates of the DNA can be amplified and sequenced clonally with a high coverage in a time-saving and cost-efficient manner. Mutations can be detected in a wildtype-background which enables the detection of minorities and is another important step towards personalized medicine.

Design: NGS was applied for a molecular screening of the complete coding region of *KRAS, BRAF, EGFR, C-KIT* and *PDGFRa* to investigate for mutations in FFPE-tumour tissue. A set of 48 CRC-FFPE-samples and a set of 48 NSCLC-FFPE-samples were analyzed. DNA was isolated and amplicon preparation (300 bp) was automated with the Fluidigm Access Array System (Fluidigm, South San Francisco, CA). Four Access Arrays were performed and multiplex Identifiers (MIDs) were added manually. After pooling and purification the pooled library was sequenced with GS-FLX (454 Life Sciences, Branford, CT, USA) with an aimed 200xcoverage.

Results: For the NSCLC-set, 544777 reads which passed filter criteria were generated with an average coverage of approximately 118x. First results show mutations in *KRAS* in the known hotspot regions in a subset of *EGFR*-negative NSCLC-patients. For the CRC-set, 720509 reads which passed filter criteria were generated with an average coverage of approximately 156x. The analysis of the data is still going on. Data for both runs will be presented.

Conclusions: The combination of the GS FLX and the Access Array System could offer a high-throughput amplicon resequencing solution applicable on DNA from FFPE-tissue. Our data suggest that NGS is a feasible method in routine molecular pathology to examine mutational status of tumour-relevant genes which are the basis for personalized medicine.

2141 Quantitative Assessment of BK Virus-Associated Nephropathy from Renal Transplant Patient Biopsies by Real-Time PCR

Y Jiang, K Muldrew. University of Toledo Medical Center, Toledo, OH.

Background: BK virus (BKV) is a member of human polyoma viruses. BK viral infection is ubiquitous in the general population and it maintains latency in renal tissues usually after a subclinical primary infection. Upon immunosuppression, BK viral infection can be reactivated and causes BKV nephropathy in renal transplanted patients. BKV nephropathy is a frequent reason for persistent graft dysfunction and frequent graft loss. As treatment for BKV nephropathy is different compared to that for renal graft rejection, it is important to have clinical assays to accurately detect active BKV infection in renal transplanted patients. Here we developed a clinical assay to evaluate BK viral load in the biopsy samples of renal transplanted patients by using real-time PCR.

Design: Sections of paraffin-embedded renal biopsy samples from renal transplant patients and autopsy kidney samples from non-transplant patients were de-paraffinized and DNA was extracted using Qiagen DNeasy Tissue Kit. Quantitative measurement of BK viral titer was made by real-time PCR assay using primers and a probe specific to the BK viral genome. Primers and probe specific to human Apolipoprotein B gene were used as internal control to normalize the sample size (number of renal cells per reaction). BK viral titers were correlated with previous immunostaining or in situ hybridization results as well as concurrent plasma BK viral load. Renal function was assessed by BUN and creatinine measurements.

Results: Significant high titer of BK viral DNA was detected in samples with previously confirmed BK viral nephropathy, whereas BK viral DNA was not detected in normal autopsy renal samples. Among BKV-positive patients, BKV was detected in renal transplant kidneys with a range of 2.82 to 4.59 $\log_{10}$ genome equivalents per cell, while concurrent plasma samples showed 5.3 to 7.5 $\log_{10}$ copies/per ml. Tissue and plasma BKV quantitation demonstrated a correlation coefficient of 0.985 for BKV-positive patients. The average serum creatinine level was 2.81 mg/dL for tissue BKV-positive patients.

Conclusions: Real-time PCR is an effective alternative approach to detect BKV infection from small kidney biopsy samples.

2142 Targeted Mutation Analysis of Endometrial Cancer Using a Custom Sequenom® MassARRAY Panel: A Proof-of-Principle Study

SE Kerr, LM Holtegaard, LM Peterson, F Medeiros, A Mariani, WE Highsmith, BR Kipp, KC Halling. Mayo Clinic, Rochester, MN.

Background: Somatic mutation analysis has become a useful tool in selecting personalized therapy for solid tumors, and may have uses for cancer screening and prognosis. As the number of gene targets increases, next-generation sequencing has been proposed as the ultimate solution to mutation detection, however, highly multiplexed targeted mutation analysis is currently more cost- and time-effective. This study explores the use of a highly multiplexed mutation detection panel designed for endometrial cancer using the Sequenom MassARRAY platform.

Design: DNA was extracted from fresh frozen (n = 75) or formalin fixed, paraffin embedded (n = 26) endometrial cancer unstained sections. Samples were subjected to a 16-well multiplexed assay targeting 19 genes and 182 mutations using PCR followed by single base extension chemistry and matrix assisted laser desorption/ionization time-of-flight detection.

Results: Mutations were detected in *PTEN* (45), *PIK3CA* (31), *KRAS* (15), *TP53* (15), *FGFR2* (7), *FBXW7* (4), *CTNNB1* (4), *NRAS* (2), *HRAS* (1), *CDKN2A* (1), and *AKT1* (1). At least one mutation was detected in 76% of the cases, and 91% of grade 1 or 2 endometrioid adenocarcinoma. The median number of mutations detected per case was 1 (range 0-4). The most frequently mutated genes are shown by histologic type in Table 1.

N Cases With Mutation (%)

Histology (n)	Any mutation	PTEN*	PIK3CA*	KRAS	TP53	FGFR2	FBXW7
Endometrioid (57)	49 (86)	28 (49)	21 (37)	11 (19)	4 (7)	6 (11)	1 (2)
Grade 1 (25)	23 (92)	15 (60)	10 (40)	6 (24)	0 (0)	1 (4)	1 (4)
Grade 2 (10)	9 (90)	7 (70)	4 (40)	1 (10)	0 (0)	3 (30)	0 (0)
Grade 3 (22)	17 (77)	6 (27)	7 (32)	4 (18)	4 (18)	2 (9)	0 (0)
Non-endometrioid (44)	28 (64)	6 (14)	8 (18)	4 (9)	11 (25)	1 (2)	3 (7)
Carcinosarcoma (20)	12 (60)	2 (10)	2 (10)	2 (10)	5 (25)	1 (5)	0 (0)
Serous (16)	12 (75)	2 (13)	5 (31)	1 (6)	4 (25)	0 (0)	3 (19)
Clear cell (6)	3 (50)	1 (17)	1 (17)	1 (17)	1 (17)	0 (0)	0 (0)
Mixed (2)	1 (50)	1 (50)	0 (0)	0 (0)	1 (50)	0 (0)	0 (0)
Total cases (101)	77 (76)	34 (34)	29 (29)	15 (15)	15 (15)	7 (7)	4 (4)

*11 cases had 2 PTEN mutations and 2 cases had 2 PIK3CA mutations.

Conclusions: This study reveals the spectrum and frequency of mutations observed in commonly mutated genes in endometrial cancer. Highly multiplexed assays may be a practical bridge to next generation sequencing for mutation detection. While several of the oncogenes tested have companion targeted therapies in clinical trials, the high mutation detection rate for endometrioid adenocarcinoma may make this approach useful for early detection screening methodologies. Further exploration for oncogenes that are commonly altered in high-grade cancer types is needed.

2143 RNA from Archived FFPE Blocks – A Valuable Underexploited Resource

TJ Kokkat, VA LiVolsi, M Patel, D McGarvey, MZ Islam, G Piermatteo, ZW Baloch. Cooperative Human Tissue Network (Eastern Division), Department of Pathology and Laboratory Medicine, Philadelphia, PA.

Background: Formalin Fixed and Paraffin Embedded (FFPE) tissue blocks constitute a valuable underexploited resource for molecular studies of disease. However the major limitation of FFPE samples for their use in molecular analyses is the degradation of RNA in FFPE samples. RNA Degradation can be caused 1) by various sample handling procedures prior to formalin fixation or 2) during formalin fixation which causes significant chemical modification of RNA or 3) after dehydration and paraffin-embedding where RNA continues to fragment and degrade over time.The quality of RNA can be represented either as RNA Integrity Number (RIN; Agilent Bioanalyzer) or RNA Quality Indicator (RQI; Biorad Experion) with a range of 1 to 10, representing totally degraded RNA to completely intact RNA. In FFPE samples, because RNA continues to degrade over time into small fragments, the RIN or RQI is much lower than frozen tissues. Recent improvements in the field of nucleic acid extraction as well as gene expression profiling have made it possible to study long-term archived tissues. Even a RIN of 1.4 has been successfully used for gene expression analysis. Therefore we investigated if time (in terms of years) of storage has effect on the quality of RNA on FFPE blocks. We compared RNA quality from FFPE blocks stored for 10 years, 5 years, 1 year to the blocks that have been stored for less than a year.

Design: Lung FFPE blocks (10 years, 5 years, 1 year and less than a year, n=16) were obtained from either clinically archived or the Cooperative Human Tissue Network repository. Two to four 10 um curls were cut from each block and processed using Allprep DNA/RNA FFPE Kit from Qiagen. RNA quality was investigated using automated electrophoresis. A minimum RQI of 1.4 was considered as threshold for useful RNA quality.

Results:

Table 1: RQI for blocks stored over different time periods

Years Stored	# blocks analyzed	# cases >1.4 RQI	Mean ± S.D	Range
10 years	5	4	2.30 ± 1.10	1.0 -3.5
5 years	4	3	2.43 ± 1.55	1.0- 4.6
1 year	3	3	1.80 ± 0.00	Not Applicable
less than 1 year	4	4	2.58 ± 0.61	1.9 -2.8

Analyses of average RQI for FFPE blocks stored at different time periods did not show a significant difference between the blocks that were processed within several months before analyses and that had been stored for 10 years, 5years and 1 year.

Conclusions: RNA quality obtained from older series of FFPE blocks are comparable to more recent blocks indicating that RNA preservation and quality in FFPE blocks seems to be preserved over time up to ten years.

2144 Multispectral Cytomorphometric Analysis with Receiver Operating Characteristic Analysis: A Mathematical Approach to Anatomic Pathology Applied to the Study of Barrett Esophagus

SH Lee, EE Furth. Hospital of the University of Pennsylvania, Philadelphia.

Background: In this study, we present our development of a rigorous, quantitative methodology coupled with receiver operating characteristic (ROC) analysis, a mathematical method developed from signal detection theory. We apply this method to the study of epithelium in Barrett esophagus. While nuclear morphology is the feature distinguishing reactive versus dysplastic cells, we hypothesized that quantifiable peri-nuclear characteristics, perhaps reflecting nuclear envelope biology, may also distinguish between these two cell classes.

Design: Cases were taken from surgical pathology esophageal biopsy specimens previously diagnosed by expert pathologists. Fourteen high-grade dysplasia slides and twelve negative-for-dysplasia slides were selected for initial analyses. From each hematoxylin-eosin-stained slide, multiple user-selected image frames at 40x magnification were selected to gather multispectral data in ten nanometer steps from 420 nm to 720 nm. These data cubes were then processed and analyzed against a pure hematoxylin spectrum to ascertain the optical density of hematoxylin staining in the perinuclear cytoplasm for each epithelial cell of interest. The distribution of optical density values for high-grade dysplastic cells was then compared against the distribution for negative cells. Each data set was normalized to 100. ROC analysis was used to determine the area under the curve (AUC) as a metric of this opitcal feature as a test to distinguish these two classes of cell types (AUC=1 being a perfect test, AUC=0.5 being non-descrimitory).

Results: 215 unique high-grade data cubes and 211 negative cubes, each with cell counts ranging from approximately 80-300 cells, were analyzed. The AUC was 0.5 showing no discriminatory value of this feature.

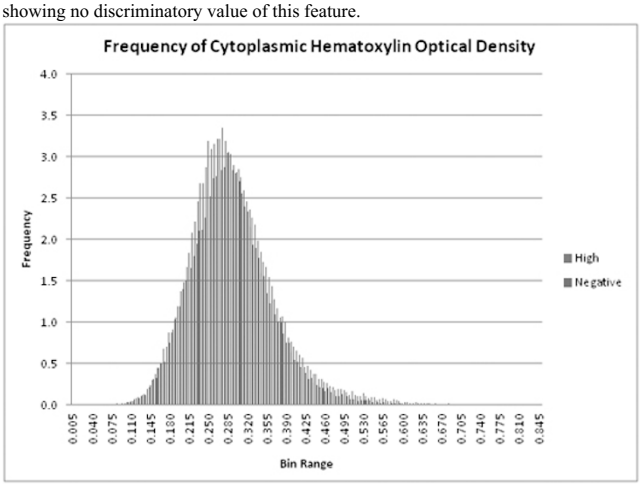

Conclusions: Multispectral cytomorphometry and the application of ROC derived from signal detection theory are powerful tools for anatomic pathology. We conclude that the perinuclear, cytoplasmic, hematoxylin optical density measurements are equivalent in benign and dysplastic epithelial cells in Barret esophagus showing that the biology of the peri-nuclear cytoplasmic environment is independent of the immediately adjacent nuclear envelope.

2145 Validation of HER2 Immunohistochemical Stain Gastric Scoring Criteria for Esophagogastric Cancer

DM Minot, HH Yoon, JS Voss, MR Henry, J Zhang, T-T Wu, RP Ketterling, AC Clayton. Mayo Clinic, Rochester, MN.

Background: New scoring guidelines have been developed and published for the interpretation of HER2 immunohistochemistry (IHC) expression in esophagogastric cancer specimens due to recognized differences in cell morphology and tumor heterogeneity. The purpose of this study is to assess the accuracy of these guidelines performed manually in comparison to image analysis (Aperio) and the established CAP/ASCO HER2 breast scoring guidelines using fluorescence in situ hybridization (FISH) as a gold standard.

Design: Ninety specimens were chosen for IHC and FISH analysis (42 esophageal biopsies with 5 matched resections, and 33 gastric biopsies with 10 matched resections). A total of 18 cases were excluded (15 insufficient for FISH analyses, 2 with insufficient tumor present in the block, and 1 equivocal FISH interpretation). Three pathologists reached a consensus interpretation on all cases based on gastric HER2 IHC guidelines and breast HER2 IHC guidelines. Image analysis was performed using the Aperio imaging system (Aperio Technologies, Vista, CA) on areas of highest stain intensity using default instrument cut-offs.

Results: Data from the 72 cases are shown (Table). Using the gastric criteria, there were no false negative cases (IHC negative [0 and 1+]/FISH positive) and 1 false positive case (IHC positive [3+]/FISH negative). Interpretations based on breast criteria yielded 2 false negative cases and 0 false positive cases. There were no false negative and one false positive case using image analysis, while having the fewest 2+ cases (n=7) resulting in the highest percentage of 2+ IHC cases (57%) being FISH positive. There was complete concordance (100%) for all IHC analysis methods between the 10 paired biopsy/resection specimens with sufficient tissue for FISH.

Consensus HER 2 Score Using Gastric Criteria, Breast Criteria and Image Analysis

	Consensus HER2 Score				
Scoring Method	0	1+	2+	3+	Total
Gastric IHC Criteria	41 (0)	16 (0)	9 (44)	6 (83)	72
Breast IHC Criteria	41 (0)	20 (10)	8 (50)	3 (100)	72
IHC Image Analysis	40 (0)	19 (0)	7 (57)	6 (83)	72

*Percentage of cases FISH positive in parentheses

Conclusions: Fewer cases were undercalled using gastric HER2 IHC scoring criteria or image analysis while one case was overcalled, when compared to standard breast scoring guidelines. Based on our validation study, the modification made to the scoring criteria to account for incomplete reactive membranes and tumor heterogeneity seems justified. In addition, image analysis could yield fewer equivocal cases that would be reflexed to FISH.

2146 Extraction and Molecular Screening of Decade-Old mRNA from Archived Breast Cancer Tissues

DE Nowak, LP Roquero, DA Chitale. Henry Ford Hospital, Detroit, MI.

Background: Since the explosion of molecular techniques in pathology over recent years, a common goal has been to develop retrospective studies where patient outcomes are known. Abundant formalin-fixed paraffin embedded (FFPE) material is available at any institution generally archived for decades. Extraction of amplifiable mRNA from old blocks has been a challenge and has been sporadically reported. Our aim was to test mRNA quality extracted from archived FFPE blocks from breast cancer patients, where the inherent fatty nature of the tissue impedes optimal fixation.

Design: Tumor FFPE tissues from breast cancer cases were retrieved between years 2000-2001. 34 cases were randomly selected for this pilot project based on morphological similarity and availability of tumor blocks with >75% tumor content. Total RNA was isolated (Recover-All Nucleic Acid Isolation Kit, Ambion), reverse transcribed (RT First Strand kit, Qiagen), and analyzed by real-time PCR on a Roche Lightcycler 480. Total RNA quantity was assessed on Nanodrop machine. Samples with more than 1ug of RNA yield were considered adequate for validation test with HPRT1 gene as primary screening housekeeping gene. Then the samples were run on Human Breast Cancer Signaling Array (Qiagen, PAH-131) that contained 84 key genes commonly involved in the dysregulation of signal transduction in breast cancer and 5 house keeping genes (Beta2 Microglobulin, GAPDH, HPRT1, ACTB, RPL13A). Positive calls were set at an arbitrary cycle threshold (CT) of 40 cycles.

Results: Total RNA extractions yielded 65 ng to 18.75 ug RNA in 34 samples. 26/34 cases (77%) yielded more than 1ug of RNA and all showed successful HPRT1 gene amplification. 19/26 cases were run on the cancer signaling array. All cases had the housekeeping genes consistently amplified with CT of 26.6-38.7. Eighty-four breast cancer associated genes showed CT value ranging from 12.8-39.8 with most arrays yielding at least 65% positive calls.

Conclusions: We have developed a protocol for the extraction and gene expression screening of decade old mRNA. While the cycle thresholds determined during the screen indicate either low relative expression or simply low recovery, the efficacy as a screening tool is readily apparent. Moreover, the process can go from paraffin block to usable screening mRNA expression data in a matter of a few hours. Applying this type of technology to additional breast data sets and other neoplasms will undoubtably increase the feasibility of using molecular techniques to retrieve valuable retrospective information currently locked away in every institution's FFPE storage archives.

2147 Analysis of Molecular Targets for Renal Cell Carcinoma

J Prather, S Sonawane, G Chappell, S Akkina, V Lindgren, S Setty. University of Illinois at Chicago, Chicago, IL.

Background: Increased interest has developed in elucidating the molecular processes surrounding development of renal cell carcinomas. Decreased activity of the PTEN tumor suppressor gene, which functions by antagonizing PI3K/AKT/mTOR signaling, has been implicated in tumorigenesis of clear cell renal cell carcinoma (ccRCC). The methods by which PTEN is downregulated include gene loss and aberrant phosphorylation and acetylation. Recent studies focus on the use of immunohistochemistry (IHC) to evaluate PTEN status. However, the clinical significance of IHC evaluation has yet to be proven. Determination of affected pathways in ccRCC may be important to both predict outcome and choose effective treatments, such as mTOR inhibitors, for ccRCC patients. As appropriate identification of the significant molecular characteristics of ccRCC tumors is essential, we sought to identify the relationship of PTEN IHC and fluorescence in situ hybridization (FISH) with Fuhrman grade and survival.

Design: We have constructed a tissue microarray of 139 primary RCCs including 104 ccRCCs which were characterized using light microscopy and IHC. We performed IHC (n=102) and FISH (n=34) with the Abbott Molecular PTEN probe with centromeric

repeat sequences as control to identify loss of PTEN. Cells with 20% or greater deletion of PTEN or monosomy of chromosome 10 were considered positive. The results were analyzed in comparison to Fuhrman grade and survival.

Results: Our study set demonstrated a correlation of Fuhrman grade with survival (p=<0.0001), a well known observation in the literature. Our population included 38% Caucasian, 33% African American, 23% Hispanic patients with 53% women. All Fuhrman grades were represented with 13% of cases grade 1, 49% grade 2, 27% grade 3 and 11% grade 4 tumors. Reduced PTEN IHC staining did not demonstrate any correlation with outcome (p=0.15, ns) or Fuhrman grade (p=0.71, ns). PTEN FISH showed deletion of 10q23 or monosomy 10 in 14/34 cases (no correlation with outcome (p=0.80, ns) or Fuhrman grade (p=0.23, ns)). 42% of cases with loss and only 30% of the non-loss cases were of higher Fuhrman grade (grade 3 and 4) (p=0.24, ns). Additionally, the cases with decreased IHC staining did not correlate with the cases demonstrating genetic loss.

Conclusions: In our study, PTEN IHC did not demonstrate significant associations with higher nuclear grade or poor outcome, supporting the recent hypothesis that loss of PTEN occurs early in the course of ccRCC development. However, our results suggest that FISH for loss of PTEN may be a method to identify a subset of tumors with poor outcome.

2148 Detection of *ALK* Gene Rearrangements in Pulmonary Adenocarcinoma: Assess for Typical and Atypical Abnormal Patterns

KK Reichard. University of New Mexico, Albuquerque, NM.

Background: A subset of pulmonary adenocarcinomas harbors an *ALK* gene rearrangement. The genetic alteration corresponds to an intrachromosomal rearrangement on 2p resulting in an *EML4-ALK* fusion at the molecular level. Detection of an *ALK* rearrangement is critical for treatment as an ALK targeted therapy, crizotinib, is available. When attempting to detect this rearrangement by fluorescence in situ hybridization (FISH) using an ALK break-apart probe, laboratorians must be cognizant of the typical abnormal but also potential atypical, yet still abnormal, patterns.

Design: We identified 9 cases of ALK-rearranged pulmonary adenocarcinomas detected by FISH from our files from 2010 to August 2011. FISH using an ALK break-apart probe was performed on paraffin-embedded, formalin-fixed whole tissue sections in all cases. Analysis was performed using an automated image analysis system, MetaSystems™, and verified by manual inspection. Positivity for an ALK rearrangement is defined in our laboratory as separation of the orange and green signals by at least four probe signal widths in >20% of tumor nuclei.

Results: The clinical, pathologic and genetic characteristics of our nine cases are shown in Table 1. Five of the nine cases showed "atypical", yet still abnormal, FISH patterns corresponding to an *ALK* rearrangement. These patterns include loss of the green, 5', centromeric probe (1F1O, 2F1O) or the presence of multiple copies of the rearrangement in each cell (1F2O2G).

Conclusions: Reliable detection of an *ALK* gene rearrangement in pulmonary adenocarcinoma requires knowledge of the typical expected abnormal pattern and atypical variants which correspond to the *EML4-ALK* molecular fusion. Although we evaluated only a small cohort of cases (9), we found that the majority of our cases showed an atypical scoring pattern. This is significant for ensuring the correct reporting of a result given an available targeted therapeutic agent.

2149 Diagnostic Accuracy and Efficiency of Whole Slide Digital Imaging in Medical Liver Disease

MS Ryan, ML Smith, PJ Boyer, JR Burton, SS Raab. University of Colorado, Aurora, CO; Mayo Clinic Arizona, Scottsdale, AZ; Memorial University of Newfoundland, St. John's, NL, Canada.

Background: Whole-slide digital imaging (WSDI) technology is beginning to transform the practice of surgical pathology. We evaluate the use of WSDI with simulated native and allograft liver biopsy cases in respect to diagnostic accuracy, efficiency, and clinical implications.

Design: We performed a case-control study in which a hepatic pathologist examined 50 liver core biopsies- 25 control specimens (using a light microscope) and 25 case specimens (using the Olympus VS110 virtual slide scanning system). These were consecutive cases diagnosed by that same pathologist two years previously. All cases included the initial clinical history and standard protocol panel of slides. The case and control groups were matched so that equivalent diagnoses were in each set. The pathologist rendered a diagnosis, confidence level (1= confident; 4= not confident), total time in slide examination, and limitations. The time to prepare cases for simulation was also recorded. A hepatologist then compared the original and review diagnosis to determine concordance.

Results: The number of non-concordant diagnoses in the case and control groups was 7 (2 major and 5 minimal) and 5 (1 major and 4 minimal), respectively. For the control group, the major error was a steatohepatitis case in which rare single necrotic hepatocytes were not recognized on glass slide review. For the case group, the two major errors were due to inadequate microscopic descriptions. The mean confidence level for the case and control group was 1.48 and 1.52, respectively. On average, cases re-diagnosed under the microscope took 4.4 minutes per case. The digital image slides uploaded slowly, leading to an average time of 5.48 minutes per case. The average time to scan a slide was 15 minutes, with 5 minutes of hands-on time per slide. 11% of the total slides were rescanned due to poor initial image quality.

Conclusions: Simulated medical liver disease cases using glass slides and WSDI show similar rates of correlation with original diagnoses, similar confidence levels, and a trend to longer time to completion using WSDI (not statistically significant). However, there was a significant difference in the time required in assembling the cases for simulation largely due to technical software difficulties and repeated scanning to achieve optimal images. For WSDI to continue its transformation of anatomic pathology practice, attention must be given to the technical/operational aspects of scanning.

2150 "Transparency" in Reporting of Radical Prostatectomy Specimens. A Simple Technique for Whole Mount Topographical Mapping of Tumor Burden Using Conventional Histologic Sections

R Sams, A Matoso, N Shillingford, S Chen, D Treaba, E Yakirevich, RA DeLellis, M Resnick, S Mangray. Rhode Island Hospital & Alpert Medical School of Brown University, Providence, RI.

Background: Prostate topographic mapping has been shown to have prognostic value in determining laterality of lymph node metastases in prostate carcinoma and provides useful information on cancer burden to the clinician. Utilization of this analysis is currently restricted to large centers that have availability of whole mount histology technique. This prevents widespread adaptation and limits the capacity for cross intitutional studies. We report a simple technique that is an alternative to whole mount histologic sections.

Design: On receipt, prostatectomy specimens are inked in 3 colors to denote right anterior, left anterior and posterior respectively inorder to facilitate orientation on examination of histologic sections. The specimens are transversely sectioned in 4-6 mm increments and slices photographed (Fig. A). After formalin fixation slices are submitted in halves or quarters and mapped on the photograph (Fig. A & Fig. B). Areas of carcinoma are outlined by a marking pen on each slide on review of histologic sections. Whole mount maps are obtained by tracing each prostatic section onto a plastic transparency (Fig. B) by correlating sections with the map from the photograph. Cancer burden is determined by overlaying the acquired whole mount transparency map onto a 1 or 2 mm grid (Fig. C) or by digital image analysis.

Results: The results obtained using this technique are demonstrated in the figure below.

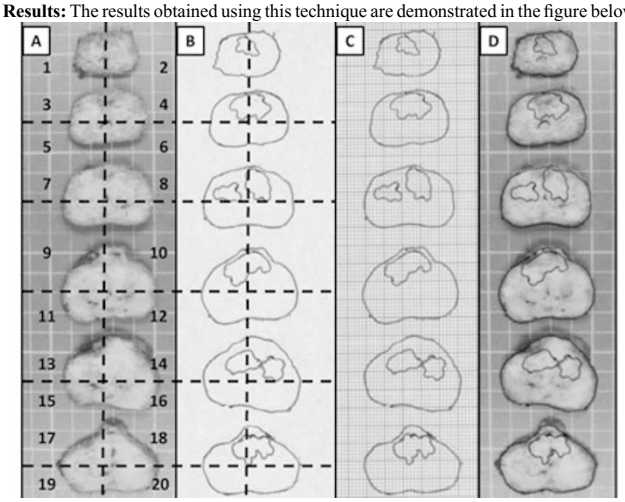

Conclusions: This alternative to whole mount histologic sections lends itself to application in any anatomic pathology laboratory and will facilitate large cross intitutional studies. These transparency maps can be overlayed onto the original photograph and incorporated into the final pathology report (Fig. D). Annotation of Gleason grade can be included as well delineation of involved margins and span of involvement. Furthermore, this method has the potential for three dimensional reconstruction similar to that done in CT imaging which can also be incorporated into the final report.

2151 Dynamic Telepatholgy-Assisted Review of Previously Misdiagnosed Frozen Sections Shows Increased Accuracy over Single Pathologist-Rendered Diagnoses

A Shah, S Sheikh-Fayyaz, T Bhuiya, NJ Morgenstern. Hofstra North Shore-LIJ School of Medicine, Lake Success, NY.

Background: Dynamic telepathology is a branch of medical telecommunications in which live video feed is transmitted in real-time from a primary location to a remote site. Our institution recently implemented this technology to transmit images of frozen sections (FZ) from two of our tertiary hospitals to our department, which has recently relocated to a centralized off-site facility, in order to assist with difficult cases in real-time. The purpose of this study is to determine whether the use of telepathology can improve FZ diagnostic accuracy within our institution.

Design: Institutional cases in which major errors were committed in original FZ diagnoses (false positives, false negatives and significant misclassification with potential for impacting patient care) over the last five years were collected. These slides were shown via telepathology to either a senior pathologist or a subspecialty service chief, as though they were real-time FZ. Original diagnoses were kept blind to both the host and the remote consultant pathologist. Telepathology-assisted diagnoses were then compared to the original FZ and final sign-out diagnoses in order to assess changes in accuracy.

Results: Forty cases were reviewed(14 pulmonary, 6 gynecologic, 6 genitourinary, 5 head and neck, 2 dermatology, 2 gastrointestinal, 2 bone & soft tissue, 1 neurology, 1 liver, 1 gallbladder). Of these, 26(65%) had improved accuracy with telepathology. Use of telepathology corrected 15 false positives and 10 false negatives. However, telepathology was unable to avoid 3 false positives and 5 false negatives. Only 1 of 5

misclassified diagnoses was improved by telepathology. Three cases (2 false negatives, 1 misclassification) were deferred by telepathology, due to suboptimal slide preparation.

Frozen Sections Shown via Telepathology

Original FZ diagnosis		Cases with improved accuracy using telepathology-assistance (%)	Cases deferred by remote telepathologist (%)
False Positives	18	15 (83)	0 (0)
False Negative	17	10 (58)	2 (12)
Misclassification	5	1 (20)	1 (20)
Total Cases	40	26 (65)	3 (7.5)

Conclusions: Our experience has shown that dynamic telepathology is an excellent tool for consultation of difficult cases, providing greater accuracy than single pathologist-rendered diagnoses. Limiting factors include suboptimal slide preparation. However, if performed in real-time, a repeat section may resolve this problem. With further experience, error compilation and training, the accuracy of telepathology-assisted frozen section diagnosis may continue to improve.

2152 Next-Generation Pathology: Deep DNA Sequencing and Targeted Therapy for Cancer

C Sheehan, A Parker, M Jarosz, S Downing, R Yelensky, D Lipson, G Palmer, M Cronin, J Ross. Albany Medical College, Albany, NY; Foundation Medicine Inc., Cambridge, MA.

Background: Gene sequencing currently used to select therapy in non-small cell lung cancer (NSCLC), colorectal cancer (CRC) and melanoma (MM) employs traditional standard-of-care (SOC) "hotspot" single gene mutation analysis. Massively parallel (next-generation sequencing (NGS)) has now been adapted to formalin-fixed (FFPE) specimens to provide high sensitivity detection for point mutations, insertion/deletions, translocations and copy number alterations (CNA).

Design: FFPE specimens from 83 solid tumors (50 CRC, 29 NSCLC, 4 MM) with results available from SOC genotyping by allele-specific PCR (KRAS codons 12/13, EGFR exons 17-20, or BRAF V600E) were fully sequenced for 145 genes by NGS. Hybridization-capture of 2574 exons across 145 oncogenes, tumor suppressor genes and ADME-related genes was performed to produce libraries appropriate for paired-end sequence analysis on the Illumina HiSeq2000 platform (Illumina, Inc., San Diego, CA).

Results: NGS recapitulated the SOC test results in all cases. In-depth sequence analysis with median coverage averaging 213-fold (range 8 to 461) detected a per-sample average of 2 previously-described mutations, 7 novel mutations and 2 CNAs in the CRC, including frequent alterations in *TP53* (33), *APC* (27), *KRAS* (12) and *BRAF* (6). The NSCLC averaged 1 previously described mutation, 8 novel mutations and 1 CNA per sample, most frequently *KRAS* (10), *TP53* (7), *JAK2* (3), *EGFR* (2) and *BRAF* (2). The MM exhibited on average 1 previously described mutation, 7 novel mutations and 3 CNAs including *TP53* (4) and *BRAF* (2). In addition to validated clinically actionable mutations in *EGFR*, *KRAS*, and *BRAF*, and multiple alterations in well-known cancer genes (*TP53, STK11*, *APC*, *MLH1, BRCA2, SMAD4)*, a significant number of additional genomic alterations that have potential therapeutic implications were also detected including activating mutations in the PI3 kinase subunit gene *PIK3CA;* mutations in *MET*, *KIT*, *ERBB2* and *CDKN2A*; driver mutations not usually associated with solid tumors, such as the lymphoma-associated *JAK2* V617F mutation in two NSCLCs; and in 1 CRC, a novel chromosome 2 rearrangement adjacent to the *ALK* kinase domain confirmed by analyzing a cDNA library constructed from extracted tumor RNA.

Conclusions: NGS of hundreds of cancer-related genes can be reliably performed at a high level of sensitivity and specificity in clinical FFPE samples of solid tumors, can reproduce SOC single gene traditional sequencing results and shows great potential to inform on therapeutic decisions for patients with CRC, NSCLC and MM.

2153 Effect of Decalcification Agents on Nucleic Acid Quantity and Quality

VM Singh, RC Salunga, YK Tran, J Gallindo, PA Plumlee, SW Chu, MG Erlander, MR Peterson. University of California San Diego, San Diego; bioTheranostics, San Diego.

Background: Molecular studies are part of standard care for cancer patients. Bone a common or sole site of metastasis requires decalcification. However commonly used decalcification agents usually contain strong acids that degrade RNA/DNA. We propose to systematically study the effect of a spectrum of commercial decalcifiers (strong acid-hydrochloric/nitric, weak acid-formic and chelating agent-EDTA) on the quantity/quality of RNA/DNA. The paradigm shift in oncology with biomarker targeted therapy and gene expression profiling studies, necessitates improved nucleic acid quality/quantity from bone.

Design: Multiple bone biopsies (obtained from amputations) of similar size and cellularity were fixed in 10% neutral buffered formalin, randomized to various decalcifiers for 2 hours then processed and embedded. Tissue lysates were obtained from unstained sections and nucleic acid isolated. DNA/RNA was quantified in nanograms by PicoGreen and RiboGreen (Life Technologies,Carlsbad,CA) respectively. Assessment of DNA/RNA integrity was accomplished by comparison of the average cycle threshold (CT) by PCR of selected housekeeping genes for each decalcifier. Results were then analyzed by two sample t-test.

Results: There was a significant decrease in both DNA/RNA yield and integrity with strong acids (hydrochloric, nitric) vs. 14% EDTA and formic acid. DNA yield was (mean ng) 5.9 vs. 37.1 (p-value 0.014) and RNA was (mean ng) 39.5 vs. 157.9 (p-value 0.002). DNA integrity was (mean CT) 38.7 vs. 28.9 (p-value 0.00004) and RNA was 34.9 vs. 26.3 (p-value 0.002). A 1-2 CT improvement for 14% EDTA and immunocal was observed.

Conclusions: The decalcification agents associated with the greatest nucleic acid quantity and better quality are 14% EDTA and formic acid decalcifiers. In addition data suggests that RNA integrity improves with 14% EDTA or immunocal.

Nucleic acid Quantity and Quality

		DNA Quantity (Picogreen)	DNA Quality (qPCR) Equal ng/reaction	RNA Quantity (Ribogreen)	RNA Quality (qRT-PCR) Equal ng/ reaction
Commercial Name	Decalcification agent	Yield (ng)	Ave CT	Yield (ng)	Ave CT
14% EDTA	14% EDTA	67.8	28.3	226.2	25.19
Immunocal	Formic acid	41.5	29.06	175.0	25.24
Surgpath decalcifier I	Formaldehyde/ Methanol/Formic acid	27.1	29.53	144.8	26.43
Formical4	Formic acid/ Formaldehyde/ EDTA	26.4	29.2	142.6	27.31
Formical2000	Formic acid/ EDTA	22.8	28.16	101.0	27.44
Nitrical	Nitric acid	11.4	39.6	51.7	31.3
IMEB HCL/Formic decal solution	HCL/Formic acid	5.8	36.37	50.4	38.8
Surgpath decalcifier II	HCL/EDTA	5.3	40.0	30.5	34.8
Decal stat	HCL/EDTA	1.4	Quantity Not Sufficient	25.4	Quantity Not Sufficient

2154 An Informatics Based Tumor Specific Data (TSD) Model with Pathology Annotations To Support Translational Research in Inter and Intra- Institutional Tumor Repositories

H Singh, W Amin, AV Parwani. University of Pittsburgh, Pittsburgh, PA.

Background: The databases model is designed to facilitate complex clinical and research functions and incorporate 'real-time' updating of information. This technically complex process required identifying the precise role of the Honest Broker and research user's interaction with data in the relational database. Our aim was to provide a simple user interface with powerful query capabilities to access de identified pathology and outcome data.

Design: The database model provides a web-based data annotation and query engine supported in a three-tiered architecture, implemented on an Oracle Application Server v10.1.2.3 running on a Windows 2007 and Oracle RDBMS v.11.1.0 running on a Community Enterprise Operating Systems (**Centos 5.3.**) virtual host definitions which is supported by IBM Cluster hardware. This model utilizes the Oracle http server and mod_plsql extensions to generate dynamic web pages. This application is flexible to facilitates investigators to search on de-identified information.

Results: This informatics supported TSD model has been in use for a decade to support translational research at local and cross institutions. An overview of the legacy database is provided briefly in the following table. This database model integrates a spectrum of data sets including clinical pathology, follow-up, molecular and imaging in relational database that allows the user to query across all types of datasets. The access to database can be regulated as per user authentication.

TSD Project List

Data Bio-repository and Project Name	Multi-institute(M) / Single Institute(S)	Total patients	Data Access :	Data Access:	Data Source
			Public or Statistical Query	User Interface (clinical and Research)	Data Annotation, Electronic data import/export
Pennsylvania Cancer Alliance Bioinformatics Consortium (Prostate, Melanoma, Breast)	M	~3000	Yes	Yes	Both
Early Detection Research Network (Colorectal and Pancreatic Virtual Biorepository)	S	2614	No	Yes	Both
SPORE (Head and Neck Neoplasm Virtual Biorepository)	S	7752	No	Yes	Both
Cooperative Prostate Cancer Tissue Resource	M	6063	No	Yes	Both
Gynecologic Cancer Research Center of Excellence	M	Under enrollment	Yes	Yes	Both

TSD Biorepository

Conclusions: The historical and current results indicate that the multi-dimensional TSD model described herein is flexible and robust and provides a highly functional solution to the pathology and research data annotation, query to accommodate research needs for critical clinical and translational research activities.

2155 Enabling Translational Research by Integrating Molecular Pathology Data with Tumor Annotation Data for Research in Head and Neck Cancers

H Singh, W Amin, AM Egloff, JR Hetrick, J Grandis, AV Parwani. University of Pittsburgh, Pittsburgh, PA; University of Pittsburgh Medical Center, Pittsburgh, PA.

Background: The SPORE Head and Neck Tumor Database is a bioinformatics supported system incorporating demographics clinical, pathological, and molecular data into a single architecture carried out by a set of common data elements (CDEs) in order to expedite head and neck cancer research. The database is built to provide semantic and syntactic interoperability of data sets and to make the data flexible, shareable and understandable across multiple systems, and end-users.

Design: The database model provides a web-based data annotation and query engine based on common data elements (CDEs) incorporated from College of American Pathologists (CAP) Checklist and North American Association of Central Cancer Registries (NAACR) standards. The system is supported in a three-tiered architecture, and implemented on an Oracle Application Server v10.1.2.3 running on a Windows 2007 and Oracle RDBMS v.11.1.0 running on a Community Enterprise Operating Systems (**Centos 5.3.**) virtual host definitions which is supported by IBM Cluster hardware. The data annotation engine is a flexible dynamic web-based tool, while the data query engine facilitates investigators to search de-identified information within the warehouse through a customizable interface.
Results: The database contains multimodal datasets that are accessible to investigators via an easy to use query tool. The database currently holds 7662 cases and provides demographic, clinical, pathology, treatment, follow-up, patient and tumor genomic sequencing and other molecular data to 12281 tumor accessions. Recent integration and link to whole genome sequence data from 92 patients is one example of how valuable such as resource of robust, highly annotated database is for researched. This database allows access to sequence analysis data set of 9423 annotation results within the same interface and flexibly accommodates additional data set needs for the future.
Conclusions: The database provides an informatics support to facilitate basic, clinical and translational science research. It offers a mechanism to efficiently select and access richly-annotated biospecimens to meet their research interests and requirements with the goal of integrating laboratory data from multiple investigators in order to develop a comprehensive characterization of individual patients and tumors. The tool protects patient privacy by providing only de-identified data with Institutional Review Board and scientific committee review and approval.

2156 SLIM as an Optical Tool To Support Pathologists in Prostate Diagnosis

S Sridharan, R Tapping, A Kajdacsy-Balla, K Tangella. Beckman Institute for Advanced Science and Technology, University of Illinois at Urbana-Champaigny, Urbana, IL; University of Illinois at Chicago, Chicago, IL; Christie Clinic and University of Illinois at Urbana-Champaign, Urbana, IL.
Background: Light microscopy is the backbone of anatomic pathology. Of the methods that could help to pathologists to obtain information beyond that obtained through usual staining methods. Spatial Light Interference Microscopy (SLIM) is an optical imaging technique that measures the phase and thus refractive index of unstained tissue. SLIM has been previously used to differentiate between benign and malignant prostate glands. In order to better evaluate SLIM as a diagnostic and prognostic tool we now attempt to use it to help recognize Gleason patterns.
Design: Using this phase map we calculated the anisotropy factor g which is the average cosine of the scattering angle associated with a single scattering event. g is related to both the variance of phase in a given tissue region and the mean value of the gradient of the phase. Two pathologists marked areas of prostate tissue microarrays where they agree on Gleason score. Anisotropy was calculated at 10X magnification.
Results: In the images obtained using SLIM, individual stromal strands can be identified. Excellent separation could be found between benign appearing and malignant areas, with a degree of accuracy of less than 1% overlap. Gleason 5 areas did not overlap with the other patterns. However, when we measured the anisotropy values for a single layer of stroma surrounding individual grade 3 and grade 4 glands in 55 tissue microarray cores with grade 3 and 33 cores with grade 4 tumor we found approximately 40% overlap. Even though the overlap precludes clinical usefulness, the mean value for anisotropy in grade 3 stroma was 0.9953, with 0.0053 SD; and for grade 4 stroma, the mean value was 0.9903 with 0.0129 SD; p-value= 0.004.
Conclusions: While SLIM is useful for differential diagnosis between benign and malignant, and also to classify Gleason grade 5 areas, additional investigation is needed in order to get a better separation between Gleason grades 3 and 4. We believe further analysis with images at 40X magnification will improve this distinction. This work will serve as background preparation in order to later address the possibility that SLIM could be used as a prognostic tool. Interestingly, the differences among Gleason grades are detectable by tissue stromal anisotropy, and not the optical properties of the epithelial component.

2157 Analysis of *IDH1* and *IDH2* Mutations in Myeloid Neoplasms Using Archived Bone Marrow Frozen Cell Pellet and Pyrosequencing Technology

N Steidler, J Gale, M Vasef. University of New Mexico, Albuquerque, NM; TriCore Reference Laboratories, Albuquerque, NM.
Background: Isocitrate dehydrogenase (*IDH*) mutations occur in 20-30% of myeloid neoplasms and are associated with a poor prognosis. In myeloid neoplasms, *IDH1* and *IDH2* mutations are often detected by Sanger sequencing or high resolution melting analysis of DNA amplified products from fresh bone marrow aspirates or formalin-fixed, paraffin-embedded tissues. We report the successful use of several years old frozen cell pellets from bone marrow monolayer cultures of myeloid neoplasms for analysis of *IDH1* and *IDH2* mutation status by pyrosequencing technology.
Design: Frozen cell pellets of bone marrow cultures stored for 4-5 years in cytogenetic freezing media were selected for this study. A total of seventy-two cases of suspected myeloid neoplasms were analyzed for *IDH1* and *IDH2* mutations. Briefly, cell pellets were thawed and then, samples treated with protein kinase buffer during white blood cell lysis, prior to DNA precipitation. After DNA isolation and polymerase chain reaction, PCR products were analyzed for mutations involving codon 132 of *IDH1* and codon 140 1nd 172 of *IDH2* by pyrosequencing.
Results: Forty-nine of 72 cases (68%) were from diagnostic pre-treatment myeloid neoplasms including AML, MDS, and MDS/MPN. The remaining 23 cases (32%) were composed of AML in remission, acute lymphoblastic leukemia, and non-specific, non-neoplastic disorders. The *IDH1* and *IDH2* mutational analysis were successful in 69/72 cases (96%). *IDH1* or *IDH2* mutations were identified in 11 out of 46 myeloid neoplasms (23%). These consisted of four *IDH1* mutations (8%) at codon 132 with substitutions of cysteine (2 cases) or histidine (2 cases) and seven *IDH2* mutations (14%) at codon 140 with substitutions of glutamine (6 cases) and codon 172 with the substitution of lysine (1 case). Eight out of 11 (72%) *IDH1* or *IDH2* mutated cases had a normal karyotype.
Conclusions: Our results indicates that the archived long term frozen bone marrow cultures are valuable resources for successful analysis of genetic abnormalities including *IDH1* and *IDH2* mutations using pyrosequencing technology. The 23% rate of *IDH1* and *IDH2* mutations in myeloid neoplasms detected in our study is comparable with previous published data. Additionally, none of the non-neoplastic samples in our study showed *IDH* mutations. This observation suggests that detection of *IDH* mutations in a borderline case may prove helpful in separating a neoplastic myeloid proliferation from a non-neoplastic process in subset of cases.

2158 Ultra-Rapid Diagnostic Tissue Preparation as an Alternative to Frozen Section

V Sujoy, C Blieden, M Garcia, SE Vernon, AR Morales. University of Miami Miller School of Medicine, Miami, FL; Jackson Memorial Hospital, Miami, FL.
Background: Hardening the tissue by freezing, which eliminates the need for fixation, processing and embedding, was introduced as a method for intra-operative pathologic consultation by Louis B Wilson at the Mayo Clinic in 1905. Because of artifacts induced by freezing tissue these intra-operative diagnoses are not uncommonly discordant with that provided by preparation of paraffin embedded blocks from the same frozen tissue (necessary to confirm the pathologic diagnosis rendered during surgery, and also for laboratory accreditation). We sought to determine if modifying conventional histological procedures could allow preparation of H&E sections from paraffin blocks in less than 20 minutes from receipt of tissue in the laboratory.
Design: We developed new tools and grossing procedures to facilitate very thin slicing of fresh tissue, designed a chemical admixture of a ketone, mineral oil and surfactant to use during grossing and microwave-based processing for 8-10 minutes (Sakura's Xpress 50), and modified procedures to shorten paraffin embedding, microtomy, staining and coverslipping to no more than 7 minutes instead of more than 30minutes as is customary. Fresh samples from a variety of different residual tissues and diseases were subjected to this novel tissue preparation method. In addition to H&E, panels of most common histochemical and immunohistochemical stains were done.
Results: The histomorphology of H&E stains obtained with this system is indistinguishable from conventional diagnostic tissue preparation. Moreover, histochemistry and immunohistochemistry results are similar, if not identical, to those obtained with formalin-fixed conventionally processed tissues.
Conclusions: Tissue sections from blocks prepared with this system have morphologic characteristics of similar or identical quality when compared with paraffin blocks prepared by conventional processing. This is a significant improvement over examination of a conventional frozen section, does not suffer from the morphologic artifacts of the latter, precludes the need to process previously frozen tissue and provides intra-operative "permanent section" diagnosis. Moreover, preliminary studies suggest that the preservation of RNA in paraffin blocks obtained with this system is similar to that from fresh frozen tissue.

2159 Neither Brief Formalin Fixation nor Rapid Tissue Processing Impact the Sensitivity of ER Immunohistochemistry in Core Biopsies of the Breast

V Sujoy, M Nadji, AR Morales. University of Miami, Jackson Health System and Sylvester Cancer Center, Miami, FL.
Background: The ASCO/CAP guidelines for estrogen receptor immunohistochemistry (ER-IHC) recommend a minimum of 8 hour formalin fixation for core breast biopsies. A number of recent publications however, have questioned the supporting evidence for this recommendation (*Gown AM; 2009, Ibarra JA et al; 2010, Apple S et al; 2011*). In this study we investigated whether brief formalin fixation and rapid tissue processing have negative effects on the sensitivity of the ER-IHC in core biopsies of the breast.
Design: Twenty-two cases of total or partial mastectomy samples were collected within 30 minutes of excision for this study. A 1.0 x 1.0 x 0.2 cm slice of each tumor was removed and further subdivided into five 1.0 x 0.2 x 0.2 cores. The cores were immediately fixed in phosphate buffered formalin solution for different period of times in the following manner: core 1 was fixed for 30 minutes, core 2 for 60 minutes, core 3 for 24 hours, core 4 for one week and core 5 was fixed in parallel with the routine surgical pathology specimens for a period of time between 12 to 48 hours. Cores 1 through 4 were processed in a formalin-free microwave-based rapid tissue processing system (Xpress, Sakura Finetek) while core 5 was processed overnight (10 hours) in a conventional tissue processor (VIP, Sakura Finetek). Immunohistochemistry for ER was performed following heat-induced antigen retrieval using monoclonal antibody ID5 and the FLEX polymer detection systems (Dako). The percentage of positive cells and the intensity of reaction was recorded for all cores.
Results: Of the total of 22 samples, five cases were ER-negative in all five cores. In 17 ER-positive cases, the reaction was present in more than 80-90% of tumor cells in each core. There was no significant differences in intensity of ER-IHC between 30 minutes, 60 minutes, 24 hours and one week formalin fixation (*Kappa=0.97*). Similarly, no difference was observed in the intensity of reaction between rapidly and conventionally processed tumors.
Conclusions: Brief formalin fixation, as short as 30 minutes, has no deleterious effect on the sensitiviy of ER-IHC in core biopsies of the breast. Furthermore, there is no significant difference between conventional overnight processing and rapid tissue processing in the sensitivity of ER immunostaining. The combination of short fixation time and rapid processing platforms enable the laboratories to significantly decrease the turnaround time for breast core biopsies.

2160 Is ER Immunohistochemical Sensitivity Affected by Different Breast Biopsy Techniques with Differing Cold Ischemia Times?

V Sujoy, A Pinto, AP Romilly, M Jorda, CR Gomez-Fernandez. Jackson Memorial Hospital/University of Miami, Miami, FL; Jackson Memorial Hospital, Miami, FL.

Background: When a patient has a suspicious mammographic abnormality or a palpable breast mass, the obligatory diagnostic tool is a biopsy.

Breast biopsies can be done in different ways. In our institution the three most common ways of obtaining breast biopsies are clinical (without imaging support), ultrasound-guided and stereotactic procedures. Clinical biopsies are placed immediately in formalin, ultrasound guided biopsies are placed in formalin after 5 minutes and stereotactic biopsies are placed in formalin after being radiographed which takes up to 10 minutes. Each technique entails different time delays to formalin fixation (cold ischemia time), which may affect the immunohistochemical sensitivity of Estrogen Receptor (ER) status. A positive reaction for Progesterone Receptor (PR) generally reflects a functional ER, and should be either equivalent or of lesser intensity/proportion to the positive reaction for ER. We utilized this paradigm to evaluate the expression of ER.

Design: Archival slides from formalin-fixed (6-48 hrs.) core biopsies of ER+ (1D5 DAKO)/PR+ (636 DAKO) invasive mammary carcinomas were retrieved from our files. Thirty cases were collected, clinical biopsies (10), ultrasound guided (10) and stereotactic (10).

Proportion and intensity of ER and PR were recorded using the Quick Score (Q-Score) and compared between the 3 different biopsy techniques.

Results: The clinical biopsies all had an ER Q-Score of 7 (mean=7) and a PR Q-Score ranging from 3 to 7 (mean=6.6). The ultrasound guided biopsies had an ER Q-Score ranging from 3 to 7 (mean=6.1) and a PR Q-Score ranging from 3 to 7 (mean=6.3). The stereotactic biopsies all had an ER Q-Score of 7 (mean=7) and a PR Q-Score ranging from 4 to 7 (mean=6.3).

PR had an equal or lesser Q-Score than ER in all of the clinical and stereotactic biopsy groups. In the ultrasound guided group PR had a Q-Score slightly higher than ER in 4 of 10 cases.

Conclusions: The positive reaction for ER did not differ across the 3 different technique groups with their inherent varying ischemic times of up to 10 minutes. When compared to the positive reaction for PR by Q score, ER was generally equivalent or of greater intensity/proportion. Four cases in the ultrasound group had a PR reaction with a slightly higher Q score than ER, but the difference was minimal. Therefore, ER immunohistochemical sensitivity is not affected by whether the breast biopsy is performed clinically, ultrasound guided, or by stereotactic procedure.

2161 Multiplex Analysis of Cavitronic Ultrasonic Surgical Aspiration (CUSA) Specimens Can Rapidly Detect High Level Oncogene Amplifications

LN Truong, S Patel, SS Martin, JF LeBlanc, A Nanda, ML Nordberg, ME Beckner. Louisiana State University Shreveport, Shreveport, LA; Louisiana State University Health Sciences Center - Shreveport, Shreveport, LA; Delta Pathology, Shreveport, LA; Louisiana State University Health Sciences Center-NO, Baton Rouge, LA; Delta Pathology Molecular Diagnostics, Shreveport, LA.

Background: Detection of amplified oncogenes in tumors is potentially influenced by specimen source. Two sources are commonly available from brain tumors, i.e. Cavitronic Ultrasonic Surgical Aspirations (CUSAs) and formalin-fixed, paraffin-embedded (FFPE) sections. Also, multiplex assay results are hindered by multiple comparisons when determining significance.

Design: This study evaluated CUSAs and FFPE specimens from the same brain tumors. Four glioblastomas, two lung carcinoma metastases, and an ependymoma were tested. Multiplex ligation dependent probe amplification (MLPA) assays to quantify seventy eight oncogenes were normalized by DNA from non-neoplastic brain (NB), [tumor DNA]/[NB DNA], to yield copy number (CN) ratios. Data were adjusted additionally by normal DNA values provided in MLPA kits. Also, FFPE and CUSA data were combined for probability calculations regarding amplifications.

Results: Purification of DNA from CUSAs was rapid (<2 days) versus FFPE (weeks) and yielded greater amounts in 6 of 7 tumors. Although normalized CN ratios ≥2.0 were more numerous in FFPE specimens, some were found only in CUSAs, consistent with tumor heterogeneity. Additionally, CN ratios adjusted further by normal DNA values provided in MLPA kits revealed 25 amplifications (≥ 2.0 CN ratio), with the nine high level (≥ 6.0) amplifications in FFPE also detected in CUSAs at increased levels. Only 2 of 6 mid level (≥ 3.0 & < 6.0 CN ratio) and 1 of 10 low level (≥ 2.0 & < 3.0 CN ratio) amplifications were detected in CUSAs. In *t* tests of amplified genes versus genes with normal CN ratios (≥0.75 to ≤1.5), corrections for multiple comparisons negatively impacted *p* values in both specimens. However, combined use of corrected CUSA and FFPE values yielded statistical significance in 64% of *p* values for amplifications.

Conclusions: CUSA specimens contained abundant brain tumor DNA, permitted detection of high level oncogene amplifications, and strengthened probabilities for amplifications. Possibly, whenever tumors in any body site are debulked as CUSA specimens, the DNA can be rapidly assessed for high-level oncogene amplifications and results can be used to aid statistical analyses of FFPE data from the same tumors.

2162 Automated Objective Determination of Percentage of Malignant Nuclei for Mutation Testing

H Viray, M Coulter, K Li, K Lane, C Hoyt, D Rimm. Yale University School of Medicine, New Haven, CT; Caliper Life Sciences, Hopkinton, MA.

Background: DNA mutations detected in tumors are a critical companion diagnostic test for some new targeted therapies. The accuracy of mutation detection depends on the sensitivity of the assay and on the percentage of tumor cells in the sample. Currently, the malignant cell percentage is judged by eye resulting in a large variation of estimated percentages. Our goal is to standardize this aspect of the test by generating a computer algorithm that can determine the percentage of malignant nuclei in a tumor tissue image.

Design: H&E images from colon adenocarcinoma cases were selected for algorithm development and testing. To create a criterion standard for evaluating algorithm accuracy, the nuclei in each image were classified as either malignant or benign and counted by a technician, then reviewed by a pathologist. Using inForm software (Caliper Life Sciences), we developed an algorithm to calculate the percentage of malignant cells in a single field of view based on feature extraction involving tissue stain optical densities and morphology. Example regions defining malignant and benign nuclei from 25 cases were used to train the algorithm. The algorithm was subsequently validated on a separate set of 35 images from a tissue microarray.

Results: Among the training images, the algorithm had a median deviation from the human counted percentage of malignant nuclei of 5.2%. Of the training images, 12 (48.0%) differed from the criterion standard by less than 5.0%, and 17 (68.0%) of the 25 images differed by less than 10.0%. In the validation set, the algorithm deviated from the criterion standard by a median of 6.0%. 14 (40.0%) of the validation images deviated by less than 5.0% and 25 (71.4%) deviated by less than 10.0%. All but one of the validation images differed from the criterion standard percentage of malignant cells by less than 20.0%.

Conclusions: The method represents an exploratory example with future potential to be used as a tool to assist in determining the percent of malignant nuclei present in a tissue sample. Further validation of this algorithm or an improved algorithm may have value to more accurately assess percentage of malignant cells for future companion diagnostic mutation testing.

2163 Mid-Infrared Spectroscopic Imaging for Tissue Histopathology

MJ Walsh, A Kajdacsy-Balla, R Bhargava. University of Illinois at Urbana-Champaign, Urbana, IL; University of Illinois at Chicago, Chicago, IL.

Background: Histopathology is the gold standard for disease diagnosis. Current histopathological techniques use a panel of special stains and immunohistochemistry (IHC) to assess tissue architecture, determine cell types present and to classify cancers. Mid-Infrared (IR) spectroscopic imaging is a novel approach to derive chemical images from tissues based on their inherent biochemistry.

Design: Mid-IR images were obtained from over 1,000 individual patients using breast, prostate and colon tissue microarrays. Serial sections were stained with a panel of routinely used special stains and IHC stains. A modified Bayesian classifier was built to assign image pixels to the correct cell types and make a decision on disease state.

Results: Using Mid-IR imaging coupled with the modified Bayesian classifier it is possible to segment tissues into their constituent cell types from a single unstained tissue section. Accurate cell type classification as measured by average Area Under the Curve (AUC) for each of the tissues is typically very high (AUC>0.95). Furthermore, diagnosis of normal or cancerous tissue based on cell type classification of breast, prostate and colon tissue could be shown.

Conclusions: Mid-IR imaging coupled with Bayesian classification could potentially be a very valuable tool as an adjunct to current histopathological procedures, with the ability to take a single unstained tissue section and give a decision on the cell types present and disease state. Accurate cell type and disease type classification has been demonstrated in breast, prostate and colon.

2164 Real-Time Histologic Assessment of CT-Guided Percutaneous Needle Core Biopsies of the Transplant Pancreas

R Wilcox, AD Bhave, P Gibson. Fletcher Allen Health Care (FAHC)/University of Vermont (UVM), Burlington; FAHC/UVM, Burlington.

Background: Gold standard for detecting pancreatic transplant rejection is percutaneous needle biopsy, guided by US or CT. Biopsy adequacy is defined as pancreatic samples containing at least 2 acinar tissue lobules associated with 2-3 septal areas. Although this is an effective method it is not absolute (reported yield for adequate tissue 83-90%).

Objective: To test whether real-time (RT) histologic assessment of CT-guided biopsies of allograft pancreases could improve the success rate of obtaining tissue adequate for histopathologic analysis.

Design: From 1/2009 - 10/2011 all pancreatic allograft biopsies followed the RT assessment protocol. The intervention radiologist contacted the transplant pathologist at time of biopsy. Within the IR suite the biopsy, on saline soaked telfa within a Petri dish, was assessed by standard light microscopy (stage lowered). At 4X the fresh tissue was examined for lobular acinar tissue (defined adequate). The radiologist, generally present at the microscope, was directly informed of inadequate tissue so additional passes/biopsies could be obtained. Adequate biopsies were placed into 10% buffered formalin and subsequently processed by standard techniques. Yield results were compared to 5-yr (2004-2008) data prior to study procedure.

Results: Results demonstrated that it is possible to identify pancreatic acinar lobules in fresh tissue under a standard microscope (Figure 1) with distinction from non-acinar tissue (e.g. adipose tissue, fibrosis). Adequate tissue for subsequent evaluation (H&E slides) for transplant rejection was obtained in 8/8 cases during the study period (100% yield), compared to 14/18 cases (78% yield) in 5 yrs prior.

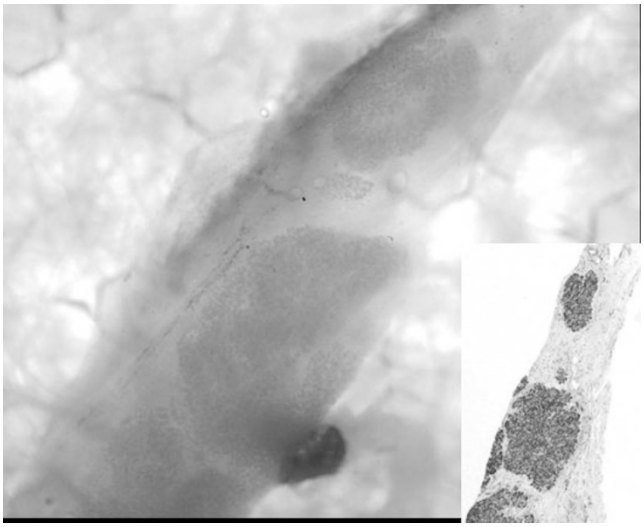

Conclusions: Obtaining pancreatic biopsies adequate for R/O transplant rejection can be difficult, especially in cases with abundant capsular reaction. Histologic assessment of fresh tissue biopsies on site can increase the rate of success, particularly in institutions that infrequently perform these biopsies. Most academic centers have a microscope available in their IR suite for evaluations of FNA specimens; therefore, this increase in yield can occur without additional cost or new equipment.

2165 Robotic MicroRNA In-Situ Hybridization by Locked Nucleic Acid Probes with Advanced Controls

MB Yaylaoglu, SD Liu, B Petryniak, AM Jubb, N Ge, G Eichele, H Koeppen. Genentech Inc., South San Francisco, CA; Max Planck Institute of Biophysical Chemistry, Goettingen, Germany.

Background: Resolving the spatial distribution of transcripts at the cellular level is essential to understanding the biology of microRNAs, and may assist in validating their function. However, the majority of in situ hybridization protocols for microRNAs are unable to demonstrate an adequate signal to background ratio, are not high throughput, do not use appropriate controls and cannot prevent hybridization of the probe to partially homologous off target sequences.

Design: This protocol uses locked nucleic acid (LNA) probes on a robotic platform to evaluate microRNA expression patterns via non-radioactive in situ hybridization (ISH) with two enzymatic amplification steps (catalyzed reporter deposition) to vastly increase sensitivity. In addition, this protocol introduces two novel controls.

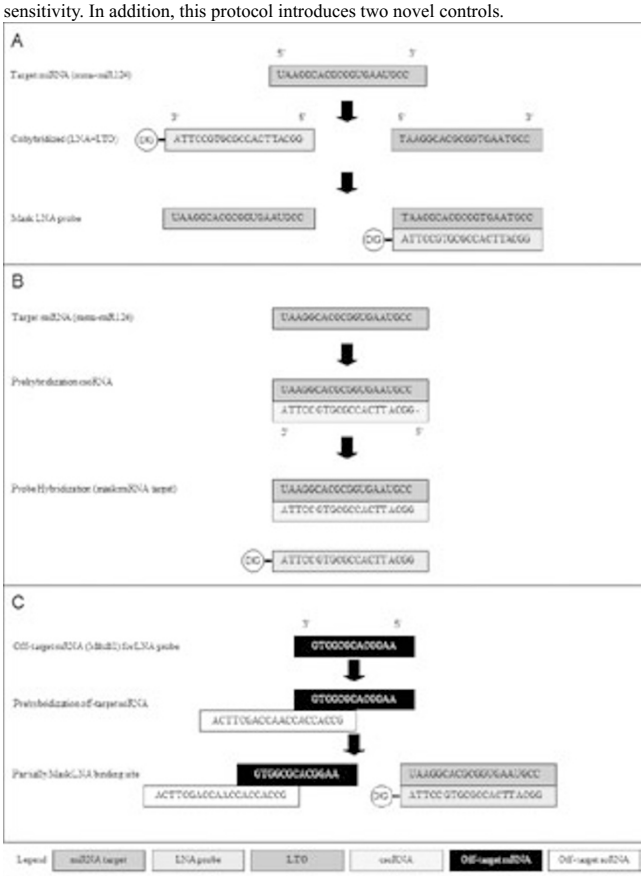

The first control is an LNA probe binding oligonucleotide, which abolishes the expression signal by trapping the LNA probe, the sequence of which is identical to that of the microRNA to be examined, termed "LTO" (LNA trap oligonucleotide). The second control comprises oligonucleotides that bind to and mask the LNA probe target sequence (that is complementary in sequence to the microRNA to be examined, termed (c)soRNA) and/or partially homologous off-target sequences, a new type of control in the form of synthetic oligomeric RNA (soRNA).

Results: We hybridized sagittal tissue sections from adult mouse brain with a LNA probe. As increasing concentrations of LTO were added the expression signal gradually decreased until it was no longer detectable.

Prehybridizing sagittal sections of adult mouse brain with increasing concentrations of csoRNA designed against the target microRNA, prevented hybridization of the LNA probe to the target.

In the presence of the cocktail, increasing csoRNA concentrations gradually decreased the specific expression signal, which was completely abolished.

Conclusions: These two controls allow us to evaluate the specificity of the LNA probe and determine whether off-target sequences exist and need to be masked, thereby increasing specificity. Proof-of-concept data are presented for mmu-miR-124 expression in mouse brain.

2166 Validation of Histology Tissue Processing and Stain Quality of Logos Rapid-Cycle Microwave Processor in Lean Continuous Flow Operations

RJ Zarbo, RC Varney, MJ Dib, B Mahar, J Wozniak. Henry Ford Hospital, Detroit, MI.

Background: Pathology report timeliness can be enhanced by technology that reduces time waste in histology. The largest delay is overnight fixation and prolonged processor times. These throughput bottlenecks can be targeted by integrating tissue processors capable of rapid-cycle times especially when aligned with continuous flow Lean work design.

Design: Evaluation of a rapid-cycle microwave processor (Logos, Milestone Medical, Kalamazoo, MI) was performed at Henry Ford Hospital Histology Core Laboratory with aims to 1) integration of processor into continuous flow work process; 2) compare specimen quality in split samples processed by conventional overnight processors and the rapid-cycle instrument. We assessed technical quality of block processing, slide cutting and H+E staining by histotechnologists and quality of H+E, special and immunohistochemical stains by pathologists with a standard input form. 238 specimens were dissected fresh and split by 2 PAs. 3 part scheme with free text comments was used for histology assessment (High, Average, Low Quality) and pathologists' microscopic evaluation (Acceptable, Inferior, Unacceptable for Diagnosis). Analysis was stratified by tissue type and processed thickness.

Results: In 238 tissues (fat, liver, placenta, ovary, colon, stomach, endometrium, cervix, ovary, uterus, prostate, testis, skin, thyroid, gallbladder, soft tissue, heart, POC, lymph node, salivary gland, thrombus, esophagus, lung, larynx), no significant quality differences were noted between rapid-cycle and conventional processors in any parameter assessed in 49 needle biopsies (1mm), 28 small biopsies (2mm) and 161 large specimens (3mm). Technical cutting quality was at variance in a minority, better in 9 cases from the rapid-cycle processor with embedded tissue being less dry or brittle whereas only 3 of the conventionally processed tissues were noted of better cutting quality. Pathologists detected no difference between the 2 types of processed specimens in any H+E stain, 10 special stains and 30 immunostains. None were of inferior technical quality for diagnosis.

Conclusions: This study validates the technical, H+E and immunohistochemical stain quality obtained with a new rapid-cycle microwave processor over a range of tissue types and processed thicknesses. The abbreviated cycle time including fixation (1.25-3 hours) facilitates the Lean approach to continuous flow processing with continuous slide production. Used in this fashion, the instrument facilitates potentially shorter report turnaround times compared to conventional overnight processing.

2167 Validation of Whole Slide Imaging for the First Line Diagnosis of Prostate Biopsies

J Zeitouni, M Jorda, C Reyes, M Nadji. University of Miami, Jackson Health System and Sylvester Cancer Center, Miami, FL.

Background: Whole slide imaging (WSI) also known as virtual microscopy is becoming an important tool in diagnostic pathology. The high resolution of images and refinement of technology now allows for WSI to be used as an alternative to conventional microscopy (CM) as a first line diagnostic platform. We investigated that possibility by comparing the intra-pathologist reproducibility of histologic diagnosis of prostate biopsies by CM and WSI.

Design: Ninety-three needle biopsies of prostate were randomly selected for this study. Each slide was scanned at 20X by BioImagene iScan Coreo Au (Ventana Medical Systems, Tucson, AZ). Four pathologists with varying degrees of experience in prostate pathology independently reviewed the glass slides first by CM, and after an interval of one week by WSI, and then a second review by CM. Diagnostic categories included benign prostatic tissue, high grade PIN, prostatic carcinoma Gleason 6, prostatic carcinoma Gleason 7 and prostatic carcinoma Gleason >7. The intra-pathologist reproducibility was recorded for CM vs WSI. Also, for each pathologist, the variation between the first CM and the second CM was used as control of the baseline. The inter-pathologist reproducibility was not the focus of this study.

Results: The intra-observer variability for CM vs WSI was 2% (observer 1), 3% (observer 2), 2% (observer 3) and 2% (observer 4). The intra-observer variability for CM vs CM was 2%, 1%, 3% and 3% for observers 1, 2, 3 and 4 respectively (*kappa=0.9875*). All intra-pathologist diagnostic disagreements (CM vs CM and CM vs WSI) were between Gleason grades 6 and 7. There were no intra-observer disagreements in the diagnosis of benign versus malignant disease or for the Gleason >7 category.

Conclusions: The intra-observer variability in the diagnosis of prostate biopsies by WSI is the same as glass slide microscopy. Our results suggest that WSI could be used as an alternative to conventional microscopy for the first line diagnosis of prostate biopsies.

2168 Could Oligonucleotide Aptamer Probe Replace Antibody for Diagnosis?

Z Zeng, P Zhang, Y Zu. The Methodist Hospital, Houston, TX.

Background: Aptamers are small molecule ligands composed of short single-stranded oligonucleotides. The high sensitivity and specificity to their targets make aptamer an excellent candidate as a diagnostic probe. In addition, aptamer probes are easily generated through chemical synthesis. However, their potential clinical value has not yet been fully explored. In this study, we tested the aptamer probes for cell immunophenotyping, tissue immunohistochemical (IHC) stain, and blood circulating tumor cell detection.

Design: For immunophenotyping a CD30-specific aptamer was synthesized and conjugated with fluorochrome. Cultured lymphoma cells were stained with aptamer probe with antibodies and analyzed by flow cytometry. For IHC study the biotinylated aptamers were used. Formalin-fixed and paraffin-embedded lymphoma tissues were stained with aptamer probes and HRP-streptavidin reporter. For circulating tumor cell detection a novel assay system was developed by conjugating aptamer probe with both fluorochrome and quencher molecule. Normally, quencher molecule interacts with fluorochrome in the same aptamer sequence and renders it inactive.

Results: 1) Flow cytometry showed that the synthetic CD30 aptamer specifically stained anaplastic large cell lymphoma and Hodgkin lymphoma cells, but not control lymphoma cells that do not express CD30 [figure1A]. Cell staining patterns of aptamer probe were identical to CD30 antibody; **2)** Tissue IHC stains showed that aptamer probe specifically recognized CD30+ lymphoma cells, but did not react to background cells in tumor sites [figure1B]. The aptamer probe could efficiently stain tissues within shorter time than standard antibody; **3)** To detect circulating tumor cells a drop of blood from lymphoma patients was simply mixed with our new assay system, in which the aptamer-mediated cell binding and subsequent intracellular internalization resulted in endosomal degradation of aptamer sequence. Separation of fluorochrome from quencher molecule present in each aptamer probe activated fluorescent signals exclusively within lymphoma cells. This one-step assay could detect single tumor cell among thousands to millions of normal blood cells with no background [figure1C].

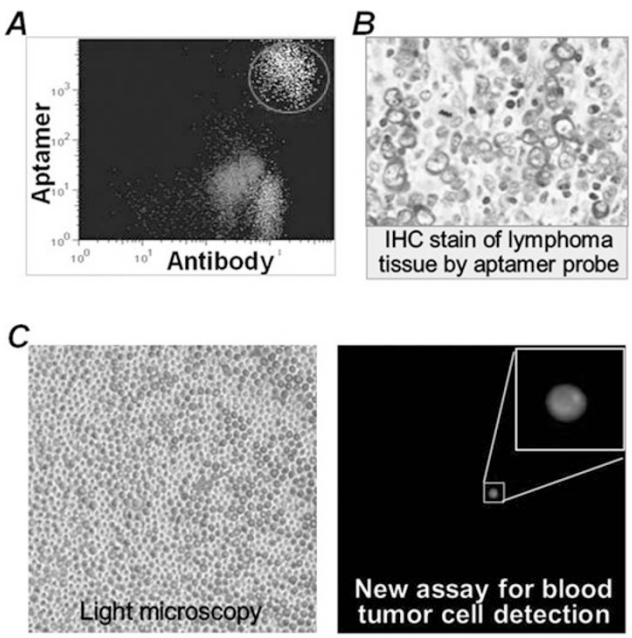

Conclusions: Our proof-of-concept studies demonstrated that the synthetic aptamer probe could replace antibody for disease diagnosis.

2169 Characteristics of Co-Amplification at Lower Denaturation Temperature-PCR (COLD-PCR) for *KRAS* Mutant Detection in Colorectal Carcinoma

S Zhang, J Tull. SUNY Upstate Medical University, Syracuse, NY.

Background: *KRAS* mutation analysis at codon 12 or 13 is important to predict response of targeted therapy against epidermal growth factor receptor (EGFR) on metastatic colorectal cancer with Erbitux. Clinical utility of regular PCR with Sanger's sequencing, a commonly used method, is limited by its low test sensitivity, i.e. 20% detection sensitivity of a mutant allele in a wild-type background. COLD-PCR provides a new approach of selective amplification on minority mutated alleles in a background of wild-type DNA. However, the characteristics of COLD-PCR plus Sanger's sequencing for *KRAS* mutation detection remains unclear in clinical samples of formalin fixed paraffin embedded tissue (FFPE).

Design: Eighteen FFPE samples of colorectal carcinoma with 10-80% tumor cellularity and known *KRAS* mutation were tested by regular PCR and COLD-PCR followed by Sanger's sequencing. The mutant to wild-type ratio between regular PCR and COLD-PCR were compared, and their correlation with tumor cellularity and variants of mutation were evaluated.

Results: The mutant/wild type ratios were generally increased in the group of COLD-PCR. However, the degree of increase was associated with mutant to wild-type ratio seen in regular PCR. When the ratios in regular PCR were ≤ 50% (8 cases), the ratios in COLD-PCR were increased by 82% on average. When the ratios in regular PCR were 50 ~ 130% (8 cases), the ratios in COLD-PCR were increased by only 19% on average. Interestingly, when the ratios in regular PCR were > 140% (2 cases), no increase or even reverse effect was observed in COLD-PCR group. Mutant/wild-type ratio was associated with tumor % cellularity only in a lower cellular group, and not related to types of *KRAS* mutation.

Conclusions: Improved *KRAS* mutant detection with COLD-PCR was demonstrated predominately in those with lower mutant/wild-type ratios, typically < 50%, in regular PCR. Through the COLD-PCR approach with Sanger's sequencing, test sensitivity for *KRAS* mutation can be elevated from 20% to 10% in general.

Ultrastructural

2170 Renal Disease with Underlying Mitochondrial DNA Mutations in Three Patients Lacking Electron Microscopic Mitochondrial Morphologic Abnormalities

LN Cossey, CP Larsen, HD Massey, TE Bunchman. University of Arkansas for Medical Sciences, Little Rock, AR; Nephropath, Little Rock, AR; Virginia Commonwealth University Medical Center, Richmond, VA.

Background: Congenital mitochondrial DNA (mtDNA) mutations are a rare cause of disease, and are often heralded by renal manifestations. Renal findings reported in association with mtDNA gene mutations vary, including nephromegaly and cyst formation grossly. By light microscopy, focal segmental glomerulosclerosis (FSGS), tubulointerstitial nephritis, and glomerular hilar hyaline lesions can be seen. And, by electron microscopy mitochondrial changes including increased numbers of mitochondria, binucleate forms, variations in size, shape and internal substructure disorganization and cristae loss are identified.

Design: Three renal biopsy specimens from patients with underlying mtDNA mutations were identified from Virginia Commonwealth University Medical Center. All biopsies were studied by light, immunofluorescence, and electron microscopy.

Results: All patients were Caucasian; two males (brothers, ages two and six) and one female (15 months). Two patients underwent percutaneous kidney biopsy, while one (s/p heart transplant) underwent autopsy. All patients were hypertensive with tubular and glomerular-based proteinuria. One patient had increased lactate levels, two patients had nephromegaly on ultrasound, and all had associated polyuria and polydipsia with normal renal function. Renal biopsies revealed focal segmental glomerulosclerosis in two patients and chronic tubulointerstitial injury/fibrosis in all patients. Electron microscopy showed intact glomerular basement membranes of appropriate thickness for age with no podocytopathy or immune complex deposits. Focal mitochondrial alterations (enlargement with substructure autolysis) consistent with fixation artifact were identified in one patient. In the remaining two patients no mitochondrial abnormalities were identified.

Conclusions: mtDNA mutations are a rare cause of renal disease and are largely undefined. In previous case series, striking electron microscopic mitochondrial and podocyte morphological changes have been associated with these mutations and described in up to 100% of study participants. Here, we have presented three mtDNA mutation patients with clinical and light microscopic changes consistent with those previously published but lacking the ultrastructural mitochondrial abnormalities which are classically described.

2171 Patterns of Proximal Tubulopathy in Monoclonal Light Chain-Associated Renal Damage Defined Ultrastructurally

GA Herrera, EA Turbat-Herrera. Nephrocor, Orlando.

Background: Proximal tubulopathy (PT) has been recognized as a pattern of renal damage in a subset of patients with circulating monoclonal light chains and renal manifestations. The clinical presentation may be sudden (acute renal failure) or slowly progressive renal dysfunction. Recognition of this entity requires careful immunomorphologic correlation.

Design: 3300 renal biopsies from 2 institutions over a period of 5 years were analyzed to identify cases of PT in patients with monoclonal light chain-associated renal dysfunction. Only those cases where the PT and related manifestations were the main pathologic findings associated with the renal damage were selected.

Specimen were examined by light, immunofluorescence, and electron microscopy with an emphasis on ultrastructural findings. Immunogold labeling, using a well described post-embedding protocol, was used in selected cases to correlate the localization of the monotypical light chains in specific compartments within the proximal tubular cells to highlight the pathologic findings.

Results: A total of 42 cases were found for a 1.6% incidence of this entity in this renal biopsy series. In all cases the proximal tubular damage was associated with monoclonal deposition of either κ or λ light chains in proximal tubules and surrounding interstitial compartment.

There were 4 distinct patterns of proximal tubular injury: 1- Tubular damage with features of acute tubular necrosis (apical blebbing, desquamation, fragmentation, vacuolization, and lysosomal proliferation in proximal tubular cells) (n=15), 2- Monotypical light chain deposition on the basolateral side associated with interstitial inflammatory response (n=21), 3- Intracytoplasmic crystalline-like inclusions in